



THE UNIVERSITY *of* EDINBURGH

Edinburgh Research Explorer

A *Miopetaurista* (Rodentia, Sciuridae) cranium from the Middle Miocene of Bavaria (Germany) and brain evolution in flying squirrels

Citation for published version:

Grau-Camats, M, Bertrand, OC, Prieto, J, López-Torres, S, Silcox, MT, Casanovas-Vilar, I & Hautier, L (ed.) 2022, 'A *Miopetaurista* (Rodentia, Sciuridae) cranium from the Middle Miocene of Bavaria (Germany) and brain evolution in flying squirrels', *Papers in palaeontology*, vol. 8, no. 4, e1454.
<https://doi.org/10.1002/spp2.1454>

Digital Object Identifier (DOI):

[10.1002/spp2.1454](https://doi.org/10.1002/spp2.1454)

Link:

[Link to publication record in Edinburgh Research Explorer](#)

Document Version:

Peer reviewed version

Published In:

Papers in palaeontology

General rights

Copyright for the publications made accessible via the Edinburgh Research Explorer is retained by the author(s) and / or other copyright owners and it is a condition of accessing these publications that users recognise and abide by the legal requirements associated with these rights.

Take down policy

The University of Edinburgh has made every reasonable effort to ensure that Edinburgh Research Explorer content complies with UK legislation. If you believe that the public display of this file breaches copyright please contact openaccess@ed.ac.uk providing details, and we will remove access to the work immediately and investigate your claim.





A *Miopetaurista* (Sciuridae, Rodentia) cranium from the middle Miocene of Bavaria (Germany) and brain evolution in flying squirrels

Journal:	<i>Palaeontology</i>
Manuscript ID	PALA-03-21-5039-OA.R2
Manuscript Type:	Original Article
Date Submitted by the Author:	29-Jan-2022
Complete List of Authors:	Grau-Camats, Montserrat; Institut Català de Paleontologia Miquel Crusafont, Universitat Autònoma de Barcelona, Paleoecology and Biochronology Bertrand, Ornella C.; University of Toronto, Scarborough, Department of Earth and Planetary Science Prieto, Jérôme; Ludwig-Maximilians-Universität München, Department für Geo- und Umweltwissenschaften, Paläontologie López-Torres, Sergi; Warsaw University Faculty of Biology, Institute of Evolutionary Biology; American Museum of Natural History, Division of Paleontology; New York Consortium in Evolutionary Primatology Silcox, Mary; University of Toronto Scarborough, Anthropology Casanovas-Vilar, Isaac; Institut Català de Paleontologia Miquel Crusafont, Universitat Autònoma de Barcelona, Paleoecology and Biochronology
Key words:	Rodentia, Sciuridae, Pteromyini, cranial morphology, endocast, encephalization quotient
<p>Note: The following files were submitted by the author for peer review, but cannot be converted to PDF. You must view these files (e.g. movies) online.</p> <p>Grau-Camats et al Appendix S1 video R2.avi</p>	

SCHOLARONE™
Manuscripts

1
2
3
4
5
6
7
8
9
10 1 ***A Miopetaurista (Rodentia, Sciuridae) cranium from the Middle Miocene of Bavaria***
11 2 **(Germany) and brain evolution in flying squirrels**

12
13
14 3 by MONTSERRAT GRAU-CAMATS¹, ORNELLA C. BERTRAND^{2*}, JÉRÔME
15 4 PRIETO³, SERGI LÓPEZ-TORRES^{4,5,6}, MARY T. SILCOX⁷ and ISAAC
16 5 CASANOVAS-VILAR^{1*}

17
18
19 6 ¹ Institut Català de Paleontologia Miquel Crusafont, Universitat Autònoma de Barcelona,
20 7 Edifici Z, Carrer de les Columnes, s/n, E-08193 Cerdanyola del Vallès, Barcelona, Spain;
21 8 montse.grau@icp.cat, isaac.casanovas@icp.cat

22
23
24 9 ² School of GeoSciences, University of Edinburgh, Grant Institute, King's
25 10 Buildings James Hutton Road, Edinburgh, EH9 3FE, UK; ornella.bertrand@ed.ac.uk

26
27
28 11 ³ Department für Geo- und Umweltwissenschaften, Paläontologie, Ludwig-Maximilians-
29 12 Universität München, Richard-Wagner-Str. 10, 80333 Munich, Germany;
30 13 j.prieto@lrz.uni-muenchen.de

31
32
33 14 ⁴ Institute of Evolutionary Biology, Faculty of Biology, Biological and Chemical
34 15 Research Centre, University of Warsaw, Żwirki i Wigury 101, 02-089 Warsaw, Poland;
35 16 s.lopez-torres@uw.edu.pl

36
37
38 17 ⁵ Division of Paleontology, American Museum of Natural History, 200 Central Park
39 18 West, 10024 New York NY, USA

40
41
42 19 ⁶ New York Consortium in Evolutionary Primatology, The Graduate Center, CUNY, 365
43 20 Fifth Avenue, 10016 New York NY, USA

44
45
46 21 ⁷ Department of Anthropology, University of Toronto Scarborough, Toronto, ON, M1C
47 22 1A4, Canada; mary.silcox@utoronto.ca

48
49
50 23 *Corresponding author

1
2
3
4
5
6
7
8
9
10 24 **Abstract:** Flying squirrels (Sciurinae, Pteromyini) are the most successful group of
11 25 gliding mammals. However, their fossil record mostly consists of isolated dental remains
12 26 which provide very limited insights into their palaeobiology and evolution. Only recently,
13 27 the first skeleton of a fossil flying squirrel, belonging to the species *Miopetaurista*
14 28 *neogrivensis*, has been described. It presents all the diagnostic gliding-related postcranial
15 29 features of its extant relatives and shows that this group has undergone very little
16 30 morphological change for almost 12 million years. However, the associated cranium is
17 31 badly crushed, so particular details of the cranial morphology cannot be described. Here
18 32 we describe a well-preserved cranium of the closely-related *Miopetaurista crusafonti*
19 33 from 12.5–12.0 Ma from Bavaria (Germany). Its cranial morphology is found to be almost
20 34 identical to extant large flying squirrels, even in details such as the position of the
21 35 foramina. The virtual endocast also shows close affinities to living large flying squirrels
22 36 in morphology and in the relative volume of different brain regions, showing diagnostic
23 37 features such as the size reduction of petrosal lobules and olfactory bulbs. However, the
24 38 encephalization quotient (EQ) and neocortical ratio are lower than observed in extant
25 39 flying squirrels. EQ is known to increase through time in squirrels, but might also be
26 40 related to locomotion, as arboreal and gliding squirrels display higher EQs than terrestrial
27 41 ones. Because *Miopetaurista* was certainly a glider, its comparatively lower EQ and
28 42 neocortical size support the existence of an independent trend of increasing EQ and
29 43 neocortical complexity in this flying squirrel subclade.

30 44 **Key words:** Rodentia, Sciuridae, Pteromyini, cranial morphology, endocast,
31 45 encephalization quotient
32 46

1
2
3
4
5
6
7
8
9
10 47 Gliding has independently evolved multiple times in mammals. There are at least two
11 48 different groups of Mesozoic gliding mammaliaforms (volaticotheres and haramyidians;
12 49 see Meng *et al.* 2006; Han *et al.* 2017; Luo *et al.* 2017), several gliding marsupials
13 50 (acrobatids, pseudocheirids, petaurids), the colugos (dermopterans), and at least four
14 51 different rodent families (Jackson 2012; Jackson & Thorington 2012). Gliding rodents
15 52 include the extant flying squirrels (pteromyins); the scaly-tailed flying squirrels
16 53 (anomalurids); at least one species of the completely extinct eomyid family from the late
17 54 Oligocene of Germany (Storch *et al.* 1996); and one extinct dormouse (glirid) species
18 55 from the Late Miocene of France (Mein & Romaggi 1991). However, of all gliding
19 56 mammals, only flying squirrels have achieved a significant diversity and wide
20 57 geographical distribution, being present in all northern continents. For a long time
21 58 considered to belong to a family or subfamily of their own (Simpson 1945; McKenna &
22 59 Bell 1997) molecular analyses have shown that they are indeed a tribe (Pteromyini) within
23 60 the Holarctic tree squirrels (Sciurinae) (Mercer & Roth 2003; Herron *et al.* 2004; Steppan
24 61 *et al.* 2004; Casanovas-Vilar *et al.* 2018; see Fig. 1). Even though transitional forms have
25 62 yet to be found, flying squirrels certainly evolved from tree squirrels and all share
26 63 specialized wrist anatomy to support and extend the patagium (Thorington 1984;
27 64 Thorington & Darrow 2000; Thorington *et al.* 2002).

28
29
30
31
32
33
34
35
36
37
38
39
40
41
42 65 Until very recently the fossil record of flying squirrels (Sciurinae, Pteromyini)
43 66 consisted solely of isolated cheek teeth and a few mandibular and maxillary fragments
44 67 (see discussion in Casanovas-Vilar *et al.* 2018). Their identification was (and for most of
45 68 them still is) controversial since many of the dental diagnostic characters used to
46 69 recognize extinct flying squirrels are also present in non-gliding species (Thorington *et*
47 70 *al.* 2005). This has led to major disagreements regarding the time of divergence and
48 71 diversification of the group. While for most mammal clades molecular-based estimates
49
50
51
52
53
54

1
2
3
4
5
6
7
8
9
10 72 yield older dates than those based on the fossil record (for example for the origin of
11 73 placental mammal orders; e.g. Springer *et al.* 2003; Bininda-Emonds *et al.* 2007; O’Leary
12 74 *et al.* 2013; Murphy *et al.* 2021), for flying squirrels fossil evidence (specifically isolated
13 75 cheek teeth belonging to the species *Hesperopetes thoringtoni*) unusually suggested a
14 76 much older divergence time (*c.* 36 Ma; Emry & Korth 2007) than most molecular
15 77 phylogenies (*c.* 23 Ma; Mercer & Roth 2003; Stepan *et al.* 2004). Contrary to dental
16 78 material, postcranial bones are unassailably diagnostic for the group since they are shaped
17 79 by the anatomical adaptations related to gliding (Thorington 1984; Thorington & Darrow
18 80 2000; Thorington *et al.* 2002, 2005). The recent description of a partial skeleton of
19 81 *Miopetaurista neogrivensis* from the Middle–Late Miocene (11.6 Ma) of Catalonia,
20 82 Spain, showed that this taxon, previously tentatively assigned to flying squirrels based on
21 83 cheek tooth morphology, displayed the gliding-related postcranial features observed in
22 84 extant forms (Casanovas-Vilar *et al.* 2018). Its diagnostic wrist anatomy further revealed
23 85 that *M. neogrivensis* belonged to the subtribe Pteromyina, which today includes large
24 86 flying squirrels, implying that the two flying squirrel subtribes (Pteromyina and
25 87 Glaucomyina) had already diverged at that time (Fig. 1). Moreover, it allowed for a
26 88 recalibration of estimates of flying squirrel divergence time, resulting in an older time
27 89 frame (late Oligocene, 31–25 Ma instead of 25–20 Ma). This new estimate is further
28 90 consistent with the age of some of the oldest purported pteromyinan fossils. Perhaps even
29 91 more importantly, this fossil showed that flying squirrels are a morphologically
30 92 conservative group. Total evidence phylogenetic analyses recognized *Miopetaurista* as
31 93 the sister taxon of the extant giant flying squirrel (*Petaurista*; Casanovas-Vilar *et al.* 2018;
32 94 see Fig. 1), with the two genera showing numerous similarities in cranial morphology and
33 95 a virtually identical postcranial anatomy. The only marked differences were found in the
34 96 cheek tooth morphology, but the striking morphological similarities in the postcranial

1
2
3
4
5
6
7
8
9
10
11
12
13
14
15
16
17
18
19
20
21
22
23
24
25
26
27
28
29
30
31
32
33
34
35
36
37
38
39
40
41
42
43
44
45
46
47
48
49
50
51
52
53
54
55
56
57
58
59
60

97 skeleton show that giant flying squirrels have undergone little evolutionary change for at
98 least 12 million years so they could be well regarded as ‘living fossils’. Phylogenetic
99 analyses combining morphological and molecular data showed that flying squirrels
100 radiated during the Miocene (mostly between 18 and 15 Ma; Casanovas-Vilar *et al.* 2018),
101 with several genera reported from Eurasia and North America (Jackson & Thorington
102 2012; Casanovas-Vilar *et al.* 2018). However, the attribution of all these taxa to the flying
103 squirrel clade (excepting *Miopetaurista*) is questionable until more diagnostic material
104 (i.e. certain postcranial elements, particularly wrist bones related to the extension of the
105 patagium) is found.

106 The remarkably complete *Miopetaurista* skeleton recently found in Catalonia
107 included an associated skull, and an additional second cranium was also recovered from
108 a nearby site. Both crania are mostly complete, but one is crushed laterally and the second
109 one dorso-ventrally, so the skull of *M. neogrivensis* was virtually reconstructed using
110 elements from both specimens that were scaled and repositioned. Even though those two
111 crania were CT-scanned, the internal morphology proved difficult to reconstruct and was
112 therefore not considered by Casanovas-Vilar *et al.* (2018). Here we describe a partial
113 cranium from the late Middle Miocene (12.5–12.0 Ma, see below) of Gumpersdorf near
114 Marktl (Bavaria, Germany) attributed to *Miopetaurista crusafonti*, a closely related
115 species. The cranial cavity was infilled with sediment, which created a natural endocast
116 that is partly exposed in the fossil. By means of CT-scanning we were able to reconstruct
117 a virtual endocast of this specimen and observe in detail endocranial morphological
118 features. Even though there are a few studies that comprehensively describe endocranial
119 morphology of some Oligocene sciurids (Bertrand *et al.* 2017, 2018), this is the first time
120 a fossil flying squirrel endocast is studied. The aims of this work are twofold. On the one
121 hand it provides an accurate description of the external and internal cranial morphology

1
2
3
4
5
6
7
8
9
10 122 for the genus *Miopetaurista* based on a well-preserved, uncrushed specimen, and thus
11 123 completing and significantly improving that of Casanovas-Vilar *et al.* (2018). On the
12 124 other hand, the endocast is accurately described and compared to that of other extant
13 125 flying squirrels to reveal if diagnostic brain features are also present. Locomotor mode
14 126 has been previously related to overall relative brain size and the size of the different brain
15 127 regions in sciurids (Bertrand *et al.* 2017, 2018, 2019a, 2021), although this is debated
16 128 because of the existence of temporal trends in relative brain size in rodents (i.e.
17 129 encephalization quotient; Bertrand *et al.* 2019a). Since *Miopetaurista* was certainly a
18 130 glider as its extant relatives, we finally discuss whether locomotion or these temporal
19 131 trends had a greater impact on brain size and in the relative size of the different brain
20 132 regions.

21 133 **MATERIAL AND METHOD**

22 134 *Material, provenance and chronology*

23 135 The described cranium (Figs 2–5; Appendix S1) was found isolated in 1978 in a gravel
24 136 quarry at the Gumpersdorf site (near Marktl, Bavaria, Germany), located in the North
25 137 Alpine Foreland Basin (NAFB) or Molasse Basin, situated on the northern side of the
26 138 Alps. The NAFB is a large foreland basin, 1000 km long by a maximum width of 130
27 139 km, that expands from western France to Austria. It formed during the uplift of the Alps
28 140 and served as a sink for the sediments eroded from that mountain range (Abdul Aziz *et*
29 141 *al.* 2010). In the German part of the basin, the sedimentary infill is divided into five main
30 142 depositional units: the Lower Marine Molasse (early and middle Oligocene); the Lower
31 143 Freshwater Molasse (late Oligocene to Early Miocene); the Upper Marine Molasse (Early
32 144 Miocene); the Upper Brackish-water Molasse (Early Miocene); and the Upper Freshwater
33 145 Molasse (OSM: Obere Süßwassermolasse; Middle to Late Miocene; Prieto & Rummel

1
2
3
4
5
6
7
8
9
10 146 2016). The Gumpersdorf site is situated in eastern Bavaria, in the OSM unit, although its
11 147 correlation to the OSM local biozones (Prieto & Rummel 2016) is uncertain. The cranium
12 148 was found 2–3 m below a marl layer, within reworked sediments, that has yielded a
13 149 diverse palaeoflora (Gregor 1982).

14
15
16
17 150 The age of these deposits is not well constrained because of the lack of
18 151 biostratigraphically informative fossils. However, Gumpersdorf had been tentatively
19 152 correlated to Mammal Neogene (MN) zone MN9 (early Vallesian, 11.2–9.9 Ma; MN zone
20 153 ranges after Hilgen *et al.* 2012) assuming a chronological proximity to Marktl, a richer
21 154 site located only a few kilometres to the south-west (Mayr 1979 and references therein).
22 155 However, recent biostratigraphic studies (Prieto & Rummel 2016) propose a late MN7+8
23 156 (late Astaracian, 13.1/12.6–11.2 Ma) age for Marktl. Another key mammal locality of the
24 157 uppermost OSM is Hammerschmide, which is correlated to the Middle–Late Miocene
25 158 boundary (11.6 Ma) on the basis of detailed bio- and magnetostratigraphic data (Kirscher
26 159 *et al.* 2016). Lithostratigraphic data indicate that Gumpersdorf is a little older than both
27 160 Marktl and Hammerschmiede, so an age of 12.5 to 12.0 Ma seems a realistic
28 161 approximation. Therefore, the Gumpersdorf specimen is slightly older than the skeleton
29 162 of *M. neogrivensis* recovered at Abocador de Can Mata site ACM/C5-D1 (Casanovas-
30 163 Vilar *et al.* 2018).

31
32
33
34
35
36
37
38 164 This specimen was briefly described and figured by Fahlbusch (1979) who
39 165 tentatively attributed it to *Miopetaurista crusafonti*. It is curated in the SNSB-Bayerische
40 166 Staatssammlung für Paläontologie und Geologie, (Munich, Germany) with collection
41 167 number 1978 V 1.

42 43 44 45 46 47 48 49 168 *Three-dimensional data acquisition and reconstruction*

50
51 169 The specimen was scanned using a Nanotom M (Phoenix X-ray) micro-CT scanner at the
52 170 Staatliche Naturwissenschaftliche Sammlungen Bayerns – Zoologische Staatssammlung

1
2
3
4
5
6
7
8
9
10 171 Museum (Munich, Germany). Scanning parameters used were 130 kV and 120 mA,
11 172 including 1505 slices with a voxel size of 32 μm . Raw data were imported to Avizo v8.0.1
12 173 software for segmentation and visualization. Cranial bones and endocast were segmented
13 174 separately using semiautomatic thresholding tools to remove sediment and bone,
14 175 respectively (Figs 4–5).

15
16
17
18
19 176 *Comparative sample*

20
21 177 Cheek teeth measurements of the studied specimen were compared to those of other
22 178 *Miopetaurista* species taken from the literature (Table 1; Grau-Camats *et al.* 2022, table
23 179 S1). Cranial anatomy and measurements were compared to original specimens
24 180 (IPS56468h, IPS88677) and to the virtual reconstruction of *M. neogrivensis* (Casanovas-
25 181 Vilar *et al.* 2018: Fig. 4B) as well as to a representative sample of extant flying squirrels
26 182 (Fig. 6, Table 2). These comprise the extant Pteromyina *Petaurista petaurista* (ZMA
27 183 131418), *Eupetaurus cinereus* (RMNH 19524), *Aeromys tephromelas* (24670), *Belomys*
28 184 *pearsonii* (RMNH 56.046) and *Pteromys volans* (RMNH 40035), and the extant
29 185 Glaucomyina represented by *Hylopetes sagitta* (RMNH 15512), *Glaucomys volans*
30 186 (RMNH 19786), *Glaucomys sabrinus* (IPS60584) and *Iomys horsfieldii* (RMNH 15937).
31 187 All specimens of the extant species are housed in the Naturalis Biodiversity Center
32 188 (Leiden, the Netherlands), except for *G. sabrinus* which comes from the collections of
33 189 the Institut Català de Paleontologia Miquel Crusafont (ICP). The *M. neogrivensis* original
34 190 specimens are also curated at the ICP.

35
36
37
38
39
40
41
42
43
44
45
46
47 191 The virtual endocast of *M. crusafonti* (Fig. 7) was compared to already published rodent
48 192 endocasts (Bertrand *et al.* 2016a, 2017, 2018, 2019b; Bertrand & Silcox 2016; Grau-
49 193 Camats *et al.* 2022, tables S2–S4; Fig. 8). These include two extant flying squirrels
50 194 belonging to different subtribes: *Pe. petaurista* (USNM 589079; Fig. 8A) and *G. volans*

1
2
3
4
5
6
7
8
9
10 195 (AMNH 240290; Fig. 8B). Extinct squirrels are represented by *Cedromus wilsoni*
11 196 (Cedromurinae; USNM 256584; Fig. 8C) from the Orellan (late Oligocene) of the White
12 197 River Formation (Wyoming, USA); and the early tree squirrel *Protosciurus cf. rachelae*
13 198 (Sciurini, Sciurinae; YPM 14737; Fig. 8D) from late early Arikareean (late Oligocene–
14 199 early Miocene) of the John Day Formation (Oregon, USA). The ischyromyid *Paramys*
15 200 *delicatus* (Paramyinae; AMNH 12506; Fig. 8E) from the Bridgerian (middle Eocene) of
16 201 the Wind River Formation (Wyoming, USA) as well as other previous published virtual
17 202 endocasts of Ischyromyidae are also included (Bertrand *et al.* 2019b). The inclusion of
18 203 ischyromyids in our study is crucial. Phylogenetic relationships among the Ischyromyidae
19 204 and with other rodent groups are still debated, but *Paramys* is generally regarded as one
20 205 of the most basal rodents (e.g. Korth 1994; Meng *et al.* 2003; Asher *et al.* 2019). Indeed,
21 206 this group of rodents has a conservative endocranial morphology (Bertrand *et al.* 2019a)
22 207 and is therefore a good representation of the plesiomorphic state for rodents and in this
23 208 case for squirrels. Aplodontiidae, is the sister group to Sciuridae (e.g. see Fabre *et al.*
24 209 2012), for which fossil endocasts are known. However, these belong to *Prosciurus*
25 210 (Bertrand *et al.* 2018) and *Mesogaulus* (Bertrand *et al.* 2021), dating back to the
26 211 Oligocene and Early Miocene, respectively, and are already too derived to provide
27 212 information on the ancestral condition from which sciurids evolved, so they are not
28 213 considered here. Phylogenetic relationships among the considered taxa, as well as their
29 214 age is illustrated in Fig. 1.

215 *Anatomical terminology and measurement methods*

216 Dental terminology and measurement methods for squirrel cheek teeth follow Casanovas-
217 Vilar *et al.* (2015) and references therein. For cranial anatomy, especially cranial
218 foramina, Wahlert (1985, 2000), Wible (2008), Sinitza *et al.* (2019) and Wible and
219 Shelley (2020) were used as primary references. The description of muscular insertion

1
2
3
4
5
6
7
8
9
10 220 areas follows Ball and Roth (1995). Linear cranial measurements are after Nicolas *et al.*
11 221 (2008) and Bertrand *et al.* (2016b) and were taken on physical specimens. Endocast
12 222 morphology as well as linear and surface measurements follow Bertrand *et al.* (2016a,
13 223 2017, 2018, 2019b) and Bertrand and Silcox (2016). Endocranial volumes and surface
14 224 areas for extant and fossil squirrels and other rodents are taken from Bertrand *et al.*
15 225 (2016a, 2017, 2018, 2019b, 2021). Endocast and brain region volumes were calculated
16 226 using Avizo v8.0.1. Because the right side of the endocast is missing a significant portion,
17 227 the total endocast volume was calculated by doubling the volume of the left half of the
18 228 endocast. The endocast exhibits some deformation, so it was divided by digitally cutting
19 229 it between the olfactory bulbs, along the superior sagittal sinus, and the midline of the
20 230 vermis in dorsal view using the ‘volume edit’ module. The neocortical surface area was
21 231 estimated by selecting the area above the orbitotemporal canal on the left side of the
22 232 endocast only, and excluding the circular fissure and the confluence of sinuses (=NS1;
23 233 following Jerison 2012; Long *et al.* 2015). The rhinal fissure represents the separation
24 234 existing between the palaeocortex and the neocortex (Martin 1990, pp 357–426). The
25 235 relationship between the rhinal fissure and the orbitotemporal canal in rodents exists as
26 236 in many other mammalian orders (e.g. lemurs; Martin 1990, pp 357–426). In the
27 237 illustration of the brain of *Sciurus vulgaris* (Brauer & Schober 1970), the rhinal fissure is
28 238 in the same location as the orbitotemporal canal in the virtual endocast of *Sciurus*
29 239 *carolinensis* (Bertrand & Silcox 2016: Fig 7c). The selected area in this hemisphere was
30 240 then doubled. Because the right side is damaged, the total endocranial surface (TS), which
31 241 includes the olfactory bulb length (see Bertrand & Silcox 2016) was estimated by using
32 242 the left side only as well and doubling it. Volume and surface area ratios are expressed as
33 243 percentages.

34
35
36
37
38
39
40
41
42
43
44
45
46
47
48
49
50
51
52 244 *Body mass and encephalization quotient estimations*

1
2
3
4
5
6
7
8
9
10 245 Body mass (BM) was estimated using a linear regression of body mass vs. cranial length
11 246 computed with the software R version 4.0.2 (R Core Team 2020) following the methods
12 247 of Bertrand *et al.* (2016a). The encephalization quotient (EQ) was used to compare
13 248 endocranial volume among species with different body masses. The EQ equation used
14 249 [EQ = 0.0097 (BM)^{0.06419}] was the one proposed by Pilleri *et al.* (1984), which is
15 250 specifically adapted to rodents. Statistical tests and plots were made using R version 4.0.2
16 251 (R Core Team 2020). For comparison purposes, we included the EQ produced by
17 252 Eisenberg and Wilson (1978).

253 *Phylogenetic signal analysis*

254 We performed regressions on the endocranial data using Phylogenetic Generalized Least
255 Squares (PGLS) regressions (Grafen & Hamilton 1989). The regressions were calculated
256 and plotted using R version 4.0.2 (R Core Team 2020). To perform the PGLS analyses,
257 we used the tree topology proposed by Bertrand *et al.* (2021), based on Korth and Emry
258 (1991) and Mercer and Roth (2003), with the addition of *M. crusafonti* as sister taxon of
259 *Petaurista* following Casanovas-Vilar *et al.* (2018). The phylogenetic tree used is given
260 in Fig. 1. We used Bayesian method to time calibrate our tree with the function
261 createMrBayesTipDatingNexus in the paleotree package v3.3.25 (Bapst 2012) and
262 followed the protocol of Bapst (2013, 2014) to create a script that was subsequently ran
263 in the software MrBayes (v3.2.7; Huelsenbeck & Ronquist 2001; Ronquist &
264 Huelsenbeck 2003). We employed the gls function of the nlme package (v3.1-142) to run
265 the PGLS analysis (Pinheiro *et al.* 2020) and used the Lambda model (Brownian motion
266 with internal branches multiplied by Pagel's λ [lambda]; Pagel 1999). We obtained a total
267 of six final PGLS regressions: (1) endocranial volume in relation to body mass, (2)
268 petrosal lobule volume in relation to body mass, (3) olfactory bulb volume in relation to
269 body mass, (4) neocortex surface area in relation to endocranial surface area, (5) petrosal

1
2
3
4
5
6
7
8
9
10 270 lobule volume in relation to endocranial volume, (6) olfactory bulb volume in relation to
11 271 endocranial volume. We computed Pagel's λ (Pagel 1999) for each PGLS regression, a
12 272 scaling coefficient that detects whether the shared evolutionary histories as specified by
13 273 the phylogeny are responsible for the patterns of similarity observed in the data. Values
14 274 below 1 correspond to traits being less similar amongst species than expected from their
15 275 phylogenetic relationships, while values above 1 suggest the reverse. We also provide the
16 276 95 % confidence intervals for each PGLS regression following the recommendations
17 277 from Symonds & Blomberg (2014).

24 278 We generated the predicted and residual values for each PGLS regression using
25 279 the function 'predict' and 'residuals' from the R stats package (v3.6-2). The functions
26 280 'R2.pred and 'R2.lik from the rr2 package (v1.0-2) were used to generate the coefficient
27 281 of correlation for each regression. We decided to report two different estimates of the
28 282 coefficient of correlation using the R^2 obtained from the predicted and from the residual
29 283 values. The first one is better than other R^2 estimators in determining how much variation
30 284 is explained by the model, while the second one is more useful when assessing the
31 285 significance of each variable used in the model (Ives 2019).

32 286 *Institutional abbreviations.* AMNH, American Museum of Natural History, New York,
33 287 USA; IPS, Institut Català de Paleontologia Miquel Crusafont, Sabadell, Spain; RMNH,
34 288 Naturalis Biodiversity Center, Leiden, the Netherlands; SNSB, Bayerische
35 289 Staatssammlung für Paläontologie und Geologie, Munich, Germany; USNM, National
36 290 Museum of Natural History, Smithsonian Institution, Washington, D.C., USA; YPM,
37 291 Peabody Museum of Natural History, Yale University, New Haven, USA; ZMA,
38 292 Zoological Museum of Amsterdam collection, Naturalis Biodiversity Center, Leiden, the
39 293 Netherlands.

294

295 **DESCRIPTION AND COMPARISONS**296 *Cheek tooth morphology*

297 The upper cheek teeth show smooth enamel without lophules; the ridges are relatively
298 simple and thick (Fig. 3E). The metaloph and the protoloph are parallel and do not
299 converge towards the protocone. The posteroloph and anteroloph are lower than the
300 protoloph and metaloph. The protocone is longitudinally elongated. The P4–M3 have a
301 large, antero-posteriorly elongated root under the protocone and two smaller cylindrical
302 roots below the metacone and paracone.

303 *P3*. It is small and conical, with a single cylindrical root. It has a prominent anterior cusp
304 and a posterior ridge which encloses a small basin. A small posterior cusp is present on
305 the posterior ridge.

306 *P4*. The right P4 is missing. The left one is subtriangular, longer than wide, and with a
307 well-developed anterior region. There are three main cusps: metacone, paracone and
308 protocone. The hypocone is reduced and integrated into the endoloph, although this cusp
309 is more marked than on the molars. The mesostyle is evident and closes the central valley.
310 The parastyle is labio-lingually elongated and is as large as the main cusps and only
311 slightly less prominent. There are two longitudinal spurs that weakly connect the
312 metaloph with the posteroloph. The anterior valley is relatively wide and labially open,
313 while the posterior one is very narrow.

314 *M1/M2*. Both molars are subrectangular, their width is notably greater than their length.
315 The M2 is relatively longer and squarer than the M1. Each of these molars possesses three
316 main cusps: metacone, paracone and protocone. The M1 has a diminutive mesostyle,
317 whereas it is missing in the M2. The protoloph is constricted near the point where it

1
2
3
4
5
6
7
8
9
10 318 merges with the protocone. The central valley is wide and labially open. In both molars
11 319 the metaloph shows a tiny posterior spur that just reaches the posteroloph but does not
12 320 merge with it. The anterior and posterior valleys are open, the latter being much narrower.
13 321 *M3*. It is subtriangular, with a conspicuously narrower posterior half. This tooth has two
14 322 main cusps: paracone and protocone. The metacone is reduced to a small cusp integrated
15 323 into a ridge that defines the posterolabial border of the molar. There is a highly reduced
16 324 postero-lingual valley defined by a thin and arched ridge, presumably corresponding to
17 325 the metaloph. This minute valley is partially closed by a small cingulum descending from
18 326 the labial side. As described for the other molars, the protoloph is constricted near the
19 327 point where it merges with the protocone. The anterior valley is very narrow and shallow
20 328 while the central valley is wider and deeper. Both valleys are labially open. Cheek teeth
21 329 measurements are given in Table 1 and comparisons are given in Grau-Camats *et al.*
22 330 (2022, table S1).
23
24 331 *Comparisons and species attribution.* The Gumpersdorf specimen is assigned to the genus
25 332 *Miopetaurista* because of its large size; the absence of enamel crenulations on the upper
26 333 cheek teeth; and the protoloph and metaloph of P4–M2 lacking conules and being parallel
27 334 to one another rather than lingually convergent (Mein 1970; Daxner-Höck & Mein 1975;
28 335 de Bruijn 1999). The specimen belongs to a medium-sized *Miopetaurista* species, clearly
29 336 larger than the Early Miocene species (early to middle Orleanian, MN3–MN4)
30 337 *Miopetaurista diescalidus*, *Miopetaurista dehmi* and *Miopetaurista lappi*. It further
31 338 differs from these species by the absence of a mesoloph, and from *M. diescalidus* in
32 339 particular by the different shape of the P4, which presents a characteristically reduced and
33 340 more rounded P4 (Daams 1977). In the case of *Miopetaurista gibberosa* from the Middle
34 341 Miocene (late Orleanian, MN5) of Göriach (Austria), only lower cheek teeth are known
35 342 (Daxner-Höck & Höck 2015), but these clearly belong to a smaller species. Younger

1
2
3
4
5
6
7
8
9
10 343 species include *Miopetaurista neogrivensis* (late Astaracian to early Vallesian, MN7+8–
11 344 MN9) and *Miopetaurista thaleri* (late Turolian to Villanyan, MN13–MN16), which are
12
13 345 the largest species of the genus, rivalling in size the extant giant flying squirrels of the
14
15 346 genus *Petaurista* (see Casanovas-Vilar *et al.* 2018). The material from Gumpersdorf is
16
17 347 slightly smaller than that ascribed to these two species and the shape of the P4 is more
18
19 348 triangular, being markedly narrower in its lingual part. In addition, the morphology of the
20
21 349 upper cheek teeth is more complex in *M. thaleri*, the M1/M2 always having a short
22
23 350 anterior spur in the protoloph (Mein 1970).

24 351 The Gumpersdorf material closely matches the size of the species *Miopetaurista*
25
26 352 *gaillardi* (Astaracian, MN6–MN7+8) and *Miopetaurista crusafonti* (Vallesian to early
27
28 353 Turolian, MN9–MN11), although it is closer to the latter. The former is known from
29
30 354 several sites ranging from Portugal to Turkey while the latter has previously only been
31
32 355 reported from Catalonia and southern France (Casanovas-Vilar *et al.* 2015). The
33
34 356 described material is slightly larger than *M. gaillardi*, further differing in the shape of the
35
36 357 P4, which is more triangular and presents a well-developed parastyle as in *M. crusafonti*.
37
38 358 Other aspects of the P4 morphology resemble these two species, such as the presence of
39
40 359 a pronounced mesostyle and two short posterior spurs in the metaloph directed towards
41
42 360 the posteroloph (see Mein 1970; Casanovas-Vilar *et al.* 2015). In *M. gaillardi* the P4
43
44 361 possesses an additional small cusp between the paracone and the parastyle, which is
45
46 362 absent in the Gumpersdorf material and in *M. crusafonti* (Casanovas-Vilar *et al.* 2015).
47
48 363 The size and morphology of the described material supports its ascription to *M. crusafonti*
49
50 364 as already suggested by Fahlbusch (1979), even though the M1/M2 may show a more
51
52 365 complex morphology in this species, with additional short spurs (Casanovas-Vilar *et al.*
53
54 366 2015). The P3 morphology of *M. crusafonti* is here described for the first time. As
55
56 367 compared to *M. neogrivensis* the P3 is more rounded and presents two well-defined cusps.

1
2
3
4
5
6
7
8
9
10 368 The material of Gumpersdorf confirms the occurrence of *M. crusafonti* in Germany
11 369 during the latest Middle Miocene (late Astaracian, MN7+8), being the only record of this
12 370 species in Central Europe. Younger occurrences of the genus *Miopetaurista* in Germany,
13 371 such as that from Dorn-Dürkheim 1 (early Turolian, MN11), have not been identified to
14 372 the species level but apparently correspond to a larger-sized species (Franzen & Storch
15 373 1975; Franzen *et al.* 2013).

20
21 374 *Cranial anatomy and comparisons*

22
23 375 *Description.* The cranium is short and wide (Figs 2–5 and Appendix S1). The total
24 376 estimated length of the cranium is 67.7 mm from the tip of the snout to the posterior part
25 377 of the braincase (for cranial measurements and comparisons see Table 2). The rostrum is
26 378 laterally crushed and deviated towards the right side. It is short and appears to have also
27 379 been wide, although extensive damage to this region obscures its morphology. The nasals
28 380 and premaxillary bones are crushed, and the different fragments displaced. The left
29 381 incisor is missing, but the right one is complete, with only minor damage on its tip. The
30 382 incisor is clearly orthodont and relatively slender. Only the anteriormost border of the
31 383 right incisive foramen is preserved, so it is impossible to evaluate its shape and size. The
32 384 infraorbital foramen is small and rounded. The infraorbital canal is long and opens lateral
33 385 to the rostrum. The orbital region, particularly the left side, is well preserved. The
34 386 braincase is not notably deformed or crushed but important parts are missing, particularly
35 387 in the dorsal part of the cranium (i.e. most part of the frontal and the right parietal; Figs
36 388 3, 4; Appendix S1). The zygomatic arches are broken, and only the zygomatic process of
37 389 the squamosal and the ventral half of the zygomatic plate are preserved. Most of the
38 390 occipital region is crushed, and the right half of the occipital bone is entirely absent. The
39 391 auditory bullae are missing. The brain cavity is infilled with terrigenous sediment, thus
40 392 producing an almost complete natural endocast (Fig. 3; Appendix S1).

1
2
3
4
5
6
7
8
9
10 393 In ventral view, the masseteric tubercles are bulbous and prominent (Fig. 4A).
11 394 The zygomatic plate is relatively vertical and wide as in other sciurids. A semicircular
12 395 ridge in front of the cheek teeth marks the insertion area for the anterior portion of the
13 396 buccinator muscle. The palate is not particularly wide and is pierced by an anterior pair
14 397 of posterior palatine foramina at the level of the M2. The posterior pair of posterior
15 398 palatine foramina are just tiny punctures in the maxillary bone close to the suture with the
16 399 palatine bones. The palatines are pierced by a well-developed, rounded and closed
17 400 posterior maxillary foramen just posterior to the M3. The posterior margin of the palatines
18 401 is straight but there is a short and rounded posterior nasal spine. Only the anterior part of
19 402 the pterygoid ridges is preserved but these appear to have been slightly divergent
20 403 posteriorly. The left foramen ovale is preserved. It is large, rounded and located
21 404 anteromedially to the inferred position of the auditory bulla. The lateral flange of the
22 405 pterygoid encloses the alisphenoid canal, which has moved from its original position. The
23 406 transverse canal is smaller and medial to the foramen ovale. A fragment of the
24 407 basisphenoid, a rectangular flat plate, is preserved on the left side.

25 408 In the orbital region, a rounded and relatively large sphenopalatine foramen is
26 409 clearly visible in the left side, whereas only its anterior border is preserved in the right
27 410 side (Fig. 5A). This foramen is located at the level of the anterior edge of the third molar
28 411 and is mostly included within the maxillary bone. An oval upper ethmoid foramen is well
29 412 preserved in the left frontal. The lower ethmoid foramen can only be observed in the left
30 413 frontal and it is somewhat damaged. It is much smaller than the upper foramen and it is
31 414 located more posteriorly, close to the suture with the squamosal. The posterior part of the
32 415 orbital region comprising the orbitosphenoid, as well as part of the palatine and frontal
33 416 bones is damaged, so that the optic and dorsal palatine foramina are not preserved. A
34 417 large and elliptical masticatory foramen (including the buccinator foramen) is visible on

1
2
3
4
5
6
7
8
9
10 418 both sides, although it is better preserved on the right side. Medial to the masticatory
11 419 foramen, the edge of a large sphenorbital fissure can also be recognized on the right
12 420 alisphenoid. Finally, a small and elliptical postglenoid foramen is visible just below the
13 421 posterior edge of the posterior zygomatic root. This foramen is only preserved on the left
14 422 side of the cranium.

15 423 The postorbital processes are not preserved (Fig. 4B). The interorbital distance is
16 424 relatively narrow compared to other squirrels (Table 2; see also Fig. 6). Even though the
17 425 zygomatic arch is broken, its posterior root is preserved on both sides of the cranium. It
18 426 is robust and almost horizontal (Fig. 4B). The cranial vault looks relatively convex
19 427 because most of the region of the cranium anterior to it is crushed and poorly preserved
20 428 (Fig. 5A). When considered in isolation, it appears to have been quite flat, thus resembling
21 429 *M. neogrivensis*. Only the left half of the parietal is preserved, but it shows a marked
22 430 temporal ridge for the insertion of the temporalis muscle (Fig. 4B). The posterior half of
23 431 the ridge curves medially before merging with a marked nuchal crest.

24 432 As already stated, the auditory bullae are not preserved. Furthermore, the right
25 433 half of the cranial vault is entirely missing. However, this makes it possible to observe
26 434 the petrosal, which is well preserved on the left side of the cranium (Fig. 5B; Appendix
27 435 S1). In medial view, the petrosal crest defines the posterior margin of a large middle
28 436 cranial fossa that houses the posterior part of the cerebrum (Fig. 2; Appendix S1). A short
29 437 sulcus on the inner surface of the anterior lamina of the petrosal probably only carried the
30 438 internal carotid nerve, as the proximal stapedia artery (= transpromontorial portion of the
31 439 artery in Wible 1984) is absent in modern Sciuroidea. Within the alisphenoid bone, the
32 440 large internal opening of the foramen ovale can also be observed on the anteroventral side
33 441 of this middle cranial fossa. A smaller posterior depression, the subarcuate fossa, occupies
34 442 the posterointernal side of the petrosal and would have housed the petrosal lobule

1
2
3
4
5
6
7
8
9
10 443 (= paraflocculus), part of the cerebellum (Fig. 2; Appendix S1). Ventral and anteromedial
11 444 to the subarcuate fossa there is a large internal auditory meatus, subdivided by a tiny
12 445 transverse crest, slightly more recessed than the meatus. The upper fossa of the internal
13 446 acoustic meatus, namely the superior acoustic foramen, is subdivided by an even weaker
14 447 crest perpendicular to the transverse crest. This perpendicular crest delimits an anterior
15 448 round opening into the facial canal and posteriorly a smaller superior vestibular area, as
16 449 well as a lower opening for the inferior vestibular area. The lower fossa of the internal
17 450 acoustic meatus, termed the inferior acoustic foramen, is also subdivided by a tiny ridge.
18 451 Its anterior half has a large and elliptical opening, the spiral cribiform tract. Posterolateral
19 452 to this foramen, is the much smaller foramen singulare for the posterior ampullary nerve
20 453 (branch of the vestibulocochlear nerve VIII) to the ampulla of the posterior semicircular
21 454 canal. The ridge separating the internal acoustic meatus from the subarcuate fossa
22 455 presents a tiny circular foramen, probably the vestibular aqueduct. A small foramen,
23 456 presumably corresponding to the mastoid foramen (see Wible & Shelley 2020: 6, 29), is
24 457 located posterodorsally to the subarcuate fossa. Another small foramen pointing towards
25 458 the back of the cranium is located posteroventrally to the internal auditory meatus. This
26 459 foramen probably corresponds to the hypoglossal foramen for nerve XII. Finally, two
27 460 small foramina can be observed at the back of the skull, close together and near the
28 461 occipital margin. These foramina probably correspond to two condyloid canals.

29
30
31
32
33
34
35
36
37
38
39
40
41
42
43 462 *Comparisons.* The cranium is short and wide, resembling that of the large flying squirrels
44 463 *Aeromys* and *Petaurista* (Fig. 6), further being comparable in size to *M. neogriviensis* and
45 464 *Pe. petaurista* (Table 2). The rostrum is short and was probably broad, as in
46 465 *Miopetaurista*, *Petaurista* and *Aeromys*. It exhibits orthodont upper incisors as seen in
47 466 our sample of extant flying squirrels. In palatal view, the masseteric tubercles are bulbous
48 467 and prominent, being similar to those of *Petaurista*. The zygomatic plate is similar in

1
2
3
4
5
6
7
8
9
10 468 morphology and size to that of other studied flying squirrels. The infraorbital foramen is
11 469 small and rounded as in *Petaurista*. The ridge for the insertion of the anterior portion of
12 470 the buccinator muscle is clearly marked as a semicircular scar similar in shape to that of
13 471 *Aeromys*. The palate is not particularly wide, being narrower than in Glaucomyina, such
14 472 as *Glaucomys*, *Hylopetes* and *Iomys*. The shape and width of the palate is again close to
15 473 *Petaurista*. The posterior palatine foramina are located at the M2 level, in the maxillary
16 474 bone. This resembles the condition seen in *Aeromys* whereas in other compared extant
17 475 flying squirrels the palatine foramina are located in the palatine, just in the suture with
18 476 the maxillary or immediately behind it. The palatines enclose two posterior maxillary
19 477 foramina, which differ from those of other Pteromyina. These foramina are not
20 478 completely closed in the studied *Pe. petaurista*, *Eupetaurus cinereus* and *Pteromys volans*
21 479 as well as in Glaucomyina species. *Aeromys tephromelas* and *Biwamoyopterus laoensis*
22 480 (see Li *et al.* 2019) are the only studied Pteromyina that show closed posterior maxillary
23 481 foramina, although they are more elongated in *A. tephromelas* than in *M. crusafonti*.
24 482 However, the intrageneric and intraspecific variability of this character has not been
25 483 evaluated, and the foramen is known to be closed in one species of the genus
26 484 *Biswamoyopterus* (*B. laoensis*) but not in the other two (*B. biswasi*, *B. gaoligongensis*;
27 485 see Li *et al.* 2019). *Miopetaurista crusafonti* presents a short and rounded posterior nasal
28 486 spine, similar in shape to that of *Pe. petaurista* and *E. cinereus*. The pterygoid ridges are
29 487 parallel in our sample of flying squirrels, but in *M. neogrivensis* and apparently in *M.*
30 488 *crusafonti* as well they diverge slightly posteriorly. The foramen ovale is large and
31 489 relatively close to the anterior margin of the auditory bulla, similar in size and shape to
32 490 that of large-sized flying squirrels.

33
34
35
36
37
38
39
40
41
42
43
44
45
46
47
48
49
50 491 The interorbital distance is relatively narrow as compared to our sample of extant
51 492 Pteromyina (Table 2; Fig. 6). Only *Belomys* and *Pteromys* show a similar interorbital

1
2
3
4
5
6
7
8
9
10 493 constriction, and the interorbital distance is wider in other Pteromyina including *M.*
11 494 *neogrivensis*. In the orbital region the frontal bone is pierced by an oval upper ethmoid
12 495 foramen at the level of the M3 whereas in other Pteromyina such as *Pe. petaurista* and *A.*
13 496 *tephromelas* it is more anteriorly placed, at the level of M2. Glaucomyina also have a
14 497 more anterior upper ethmoid foramen compared to *M. crusafonti*, at the M2 level. The
15 498 sphenopalatine foramen is almost entirely included within the maxillary bone, as
16 499 observed in *A. tephromelas*. However, in extant large flying squirrels, as well as in some
17 500 small taxa such as *Hylomyscus sagitta*, the position of this foramen is more anterior (at the
18 501 contact between M1 and M2) than in *M. crusafonti* (at the contact between M2 and M3).
19 502 The squamosal is relatively low and presents a small postglenoid foramen, which within
20 503 the compared specimens only occur in *Petaurista* and *Eupetaurus*.

21 504 The root of the jugal is deep and robust approaching the morphology of *Petaurista*.
22 505 On initial overview, the cranial vault of *M. crusafonti* seems relatively convex, more
23 506 closely resembling smaller-sized flying squirrels. However, the dorsal part of the
24 507 cranium, particularly the frontal, is poorly preserved thus giving this false impression of
25 508 convexity. Therefore, the morphology of the cranial vault was certainly somewhat
26 509 originally flatter, although probably not as much as in *Petaurista* or *Aeromys* species. The
27 510 preserved part of the parietal bone shows a prominent temporal ridge that curves medially
28 511 towards the nuchal crest similarly to *M. neogrivensis* and *E. cinereus*. These ridges do not
29 512 come as close towards the posterior side of the cranium in other flying squirrels, such as
30 513 in *Petaurista*, *Aeromys* or *Pteromys*.

31 514 Except for its greater interorbital constriction, the cranium of *M. crusafonti* does
32 515 not differ significantly from that of *M. neogrivensis* (Fig. 6B), hence being remarkably
33 516 similar to the large flying squirrels *Petaurista* and *Aeromys*. Yet, as remarked by
34 517 Casanovas-Vilar *et al.* (2018), the cheek tooth morphology is clearly different and there

1
2
3
4
5
6
7
8
9
10 518 are subtle cranial differences. *Miopetaurista* has the temporal ridges that converge
11 519 towards the posterior edge of the cranium, resembling the condition seen in *Eupetaurus*.
12
13 520 On the other hand, the morphology of the posterior maxillary foramina is different from
14
15 521 that of *Petaurista* and *Aeromys*, but the intrageneric and intraspecific variability of this
16
17 522 character has not been assessed, so it may not be diagnostic.

18 19 523 *Endocranial anatomy and comparisons*

20
21 524 *Olfactory bulbs.* The olfactory bulbs of *M. crusafonti* are located above the M1 (Fig. 2;
22
23 525 Appendix S1), which is different to the position observed in all fossil and extant squirrels
24
25 526 but similar to some ischyromyids (see Bertrand *et al.* 2018). It is possible that the position
26
27 527 of the olfactory bulbs could have resulted from deformation of the rostral region being
28
29 528 telescoped anteriorly compared to the braincase; however better-preserved specimens
30
31 529 will be necessary test this hypothesis. In ischyromyid rodents past studies have found that
32
33 530 the olfactory bulbs are positioned more posteriorly relative to the toothrow, above the
34
35 531 M1–M2 (Bertrand *et al.* 2016b, 2019b). This might be related to the fact the rostrum
36
37 532 appears to have shortened and the braincase expanded due to brain size increase in
38
39 533 Sciuridae compared to Ischyromyidae (Bertrand *et al.* 2019a). The olfactory bulbs
40
41 534 represent 1.2 % of the total endocranial volume in *M. crusafonti* (Grau-Camats *et al.*
42
43 535 2022, table S4). *Miopetaurista crusafonti* has a smaller olfactory bulb volume ratio
44
45 536 compared to Eocene and Oligocene Ischyromyidae (3.2 % to 6.1 %), the Oligocene
46
47 537 squirrel *Cedromus wilsoni* (3.0 %), the late Oligocene Sciurini *Protosciurus* cf. *rachelae*
48
49 538 (3.7 % and 4.9 %), and extant squirrels, which range from 1.6% to 4.7 %. *Miopetaurista*
50
51 539 *crusafonti* also has a lower ratio compared to extant flying squirrels, which range from
52
53 540 1.6 % to 3.5 % in olfactory bulb ratio (Table 3; Grau-Camats *et al.* 2022, table S4). Among
54
55 541 the considered extant squirrel sample, *Ratufa affinis* and *Pe. petaurista*, the closest living
56
57 542 relative of *M. crusafonti*, show the lowest olfactory bulb volume ratios (1.6 %). Log-

1
2
3
4
5
6
7
8
9
10 543 transformed olfactory bulb volume shows a positive and highly significant correlation
11 544 with both log-transformed endocranial volume and body size (Fig. 9A, B; Table 4). Both
12 545 endocranial volume and body mass explain a high portion of the variance according to
13 546 PGLS regression (Table 4; $r^2=0.86$ against body mass and $r^2=0.91$ against endocranial
14 547 volume). The phylogenetic signal is moderate when assessed against body mass ($\lambda\sim 0.6$)
15 548 and high ($\lambda\sim 0.9$) if endocranial volume is considered (Table 4). *Miopetaurista crusafonti*
16 549 has smaller olfactory bulbs than would be expected for its endocranial volume compared
17 550 to ischyromyids, other fossil sciurids and the majority of extant squirrels (Fig. 9A). It also
18 551 has smaller olfactory bulbs than would be expected when assessed against body mass
19 552 compared to extant sciurids (Fig. 9B). The flying squirrels *Pe. petaurista* and *Pteromys*
20 553 *buechneri* have high negative residuals and occupy a similar position relative to the
21 554 regression line for squirrels to *M. crusafonti* (Grau-Camats *et al.* 2022, tables S6–S7)
22 555 although they fall within the cluster of Ischyromyidae when the comparison is made with
23 556 respect to body mass (Fig. 9B).

24 557 *Cerebrum and midbrain.* The circular fissure (Fig. 7A; Appendix S1) of *M. crusafonti* is
25 558 shorter antero-posteriorly than in ischyromyid rodents but similar in length compared to
26 559 that of sciurids, including the extinct *C. wilsoni* and *Pr. cf. rachelae* (Fig. 8; Bertrand *et*
27 560 *al.* 2017, 2018, 2019b). The ratio of cerebellum maximum width to cerebrum maximum
28 561 width (CLW/CRMW) is variable in the studied taxa (Grau-Camats *et al.* 2022, table S3).
29 562 *Miopetaurista crusafonti* has a ratio of 65.8 %, which is very close to the value for the
30 563 early squirrel *C. wilsoni* (66.2 %) and lower than the values for the two specimens of *Pr.*
31 564 *cf. rachelae* (69.4 % and 79.27 %). The ratio of *M. crusafonti* is lower than the range
32 565 observed for extant squirrels (68.8 % to 82.4 %). This result contrasts with the condition
33 566 in ischyromyids, for which the ratio is higher, between 82.5 % and 103.6 %, suggesting
34 567 that the cerebellum and cerebrum have more similar widths in this family of early rodents

1
2
3
4
5
6
7
8
9
10 568 (Bertrand *et al.* 2019b). Previous research concluded that the lower ratio exhibited by
11 569 squirrels is explained by the lateral expansion of the cerebrum relative to the cerebellum
12
13 570 compared to the configuration in ischyromyid rodents (Bertrand *et al.* 2018, 2019b). The
14
15 571 lowest ratios in the extant dataset occur in flying squirrels, with two species displaying
16
17 572 the lowest values for extant taxa: *Hylopetes spadiceus* (68.8 %) and *Pt. buechneri*
18
19 573 (69.3%). The midbrain is not visible on the endocranial surface of *M. crusafonti*, which
20
21 574 implies complete coverage of this area by the cerebrum (Figs 7A, C). The observed
22
23 575 condition resembles all extant squirrels (e.g. Fig. 8A, B) but contrasts with the situation
24
25 576 in other extinct squirrels which exhibit only a partially covered midbrain (Fig. 8C, D;
26
27 577 Bertrand *et al.* 2017, 2019b).

28
29 578 A temporal fossa is visible in the fossil taxa *C. wilsoni* (Fig. 8C), *Pr. cf. rachelae*
30
31 579 (Fig. 8D), *M. crusafonti* (Fig. 7C) as well as in all studied extant squirrels. In contrast, the
32
33 580 fossa is absent in most ischyromyid rodents (e.g. Fig. 8E) with the exception of
34
35 581 *Pseudotomus horribilis*, *Pseudotomus hians*, one specimen of *Ischyromys typus* and in
36
37 582 *Reithroparamys sciuroides* (Bertrand *et al.* 2019b). The Sylvian fossa is absent in the
38
39 583 fossil taxa *M. crusafonti*, *Pr. cf. rachelae*, and also in the ischyromyids (Bertrand *et al.*
40
41 584 2018, 2019b). The presence of this structure is variable among other extant and extinct
42
43 585 squirrels. For instance, a Sylvian fossa is visible in *C. wilsoni* (Fig. 8C) but is absent in
44
45 586 our sample of pteromyins except for *A. tephromelas*, *Petinomys setosus* and *Pt.*
46
47 587 *buechneri*, while an actual Sylvian sulcus can be observed in the invertivorous
48
49 588 callosciurine *Rhinosciurus laticaudatus* (Bertrand *et al.* 2017). Lateral sulci are absent in
50
51 589 *M. crusafonti*, *C. wilsoni*, *Pr. cf. rachelae* and in the majority of our extant squirrel
52
53 590 sample, while the presence of lateral sulci is variable in the ischyromyids (see Bertrand
54
55 591 *et al.* 2019a). However, they are visible in large flying squirrels, such as the pteromyins
56
57 592 *A. tephromelas* and *Pe. petaurista* (Fig. 8A; Bertrand *et al.* 2017), which also have the

1
2
3
4
5
6
7
8
9
10 593 highest endocranial volumes within the Sciuridae (11.5 cm³ in *A. tephromelas* and 12.3
11 594 cm³ in *Pe. Petaurista*; Table 3; Grau-Camats *et al.* 2022, table S4). Calculated endocranial
12 595 volume for *M. crusafonti* is 10.82 cm³, thus being lower than both extant taxa. In general,
13 596 presence or absence of neocortical sulci is related to the endocranial volume, with brains
14 597 of less than 5 cm³ generally being lissencephalic (Macrini *et al.* 2007). For rodents, both
15 598 gyrencephalic and lissencephalic brains can be found in an interval of brain masses
16 599 between 3 and 30 cm³ (Pilleri *et al.* 1984). The absence of sulci in all but the largest
17 600 squirrels suggests that the value below which gyrification occurs may be higher than in
18 601 some other mammalian groups. As such, *M. crusafonti* may differ from the large extant
19 602 flying squirrels in lacking the lateral sulcus because of its somewhat smaller brain size.

20
21
22
23
24
25
26
27 603 The position of the orbitotemporal canal of *M. crusafonti* (Fig. 7C) is similar to
28 604 that of the late Oligocene sciurid *Pr. cf. rachelae* (Fig. 8D) in being near the ventral extent
29 605 of the temporal lobe. This structure is positioned more ventrally in *M. crusafonti*
30 606 compared to ischyromyid rodents and the early Oligocene sciurid *C. wilsoni* (Figs 8C, E;
31 607 Bertrand *et al.* 2017, 2019b). A ventrally positioned canal reflects a ventral expansion of
32 608 the neocortex, based on the inferred relationship between the canal and the rhinal fissure
33 609 in sciurids (Bertrand *et al.* 2017). In extant squirrels the orbitotemporal canal is even more
34 610 ventrally positioned than in *Pr. cf. rachelae* (e.g. Fig. 8A, B), thus resulting in a greater
35 611 neocortical surface area. This canal is straight in *M. crusafonti* and morphologically
36 612 similar to that of the flying squirrels *A. tephromelas* and *Pe. petaurista* (Bertrand *et al.*
37 613 2017). The neocortex of *M. crusafonti* represents 30.2% of the total endocast surface area,
38 614 which is in the range of the values obtained for other extinct squirrels (Fig. 9C, Table 3;
39 615 Grau-Camats *et al.* 2022, table S4). In extant squirrels the ratio is higher, ranging from
40 616 33.8 % to 39.3 % and for flying squirrels specifically, the range of values is between 33.8
41 617 % and 36.7 % (Fig. 9C; Table 3; Bertrand *et al.* 2017; Grau-Camats *et al.* 2022, table S4).

1
2
3
4
5
6
7
8
9
10 618 This result contrasts with ischyromyids, which range from 16.3 % to 23 % (Bertrand *et*
11 619 *al.* 2016b, 2018, 2019b). Log-transformed neocortical surface area shows a positive and
12
13 620 highly significant correlation with log-transformed endocranial surface area, the latter
14
15 621 variable explaining a significant part of existing variance ($r^2 > 0.90$; Table 4). Our analyses
16
17 622 show that phylogenetic signal is strong ($\lambda > 1$; see Table 4), which would suggest that more
18
19 623 closely related species display more similar neocortical sizes in our sample (Fig. 9D).
20
21 624 However, this result appears to be mainly driven by ischyromyid rodents as they have a
22
23 625 much lower neocortical surface area percentage compared to extinct and extant squirrels.
24
25 626 Indeed, after rerunning the PGLS analysis without Ischyromyidae, λ dropped close to 0
26
27 627 (and correlation increased to $r^2 > 0.99$; Table 4), suggesting that the impact of phylogeny
28
29 628 on the relative size of the neocortex is not strong among extinct and extant squirrels.
30
31 629 Nevertheless, the neocortical surface area in *M. crusafonti* is slightly smaller than would
32
33 630 be expected for its endocranial surface area (Fig. 9D). *Miopetaurista crusafonti* has
34
35 631 residual values from the regression line that are close to those calculated for other fossil
36
37 632 squirrels, *Pr. cf. rachelae* and *C. wilsoni* (Fig. 9D, Bertrand *et al.* 2017, 2018; Grau-
38
39 633 Camats *et al.* 2022, tables S6–S7).

40
41 634 The hypophyseal fossa is poorly defined, although there is a slight bulge in the
42
43 635 endocast just posterior to the optic chiasm that might mark its position. A poorly
44
45 636 demarcated fossa is also characteristic of *C. wilsoni* (Fig. 8C) and most extant sciurids
46
47 637 studied here, although it is more salient in some ischyromyids (e.g. Fig. 8E; Bertrand &
48
49 638 Silcox 2016; Bertrand *et al.* 2016b, 2017, 2018, 2019b).

50
51 639 *Cerebellum*. The caudal region of the endocast of *M. crusafonti* is damaged. The vermis
52
53 640 of the cerebellum is visible, separated from the left lateral lobe of the cerebellum by the
54
55 641 paramedian fissure (Fig. 7A, C; Appendix S1). Only the left petrosal lobe
56
57 642 (=paraflocculus, see Bertrand *et al.* 2020) is preserved, therefore, the volume calculated

1
2
3
4
5
6
7
8
9
10 643 for the left petrosal lobe was compared to the volume for the left side of the endocast
11 644 (Table 3; Grau-Camats *et al.* 2022, table S4). *Miopetaurista crusafonti* has relatively
12 645 smaller petrosal lobules (1.9 % of total endocast volume) compared to the other fossil
13 646 squirrels, *C. wilsoni* (3.2 %) and *Pr. cf. rachelae* (3.3 %), thus being in the range of extant
14 647 squirrels (0.9 %–2.3 %) and in the upper part of the range of ischyromyid rodents (0.4
15 648 %–2.1 %; Bertrand *et al.* 2017, 2018, 2019b). Compared to extant pteromyins, *M.*
16 649 *crusafonti* is in the upper range of variation for the petrosal lobule volume ratio (0.9 %–
17 650 1.7 %). Log-transformed petrosal lobule volume shows a positive and highly significant
18 651 correlation with both log-transformed endocranial volume and body mass. Both
19 652 endocranial volume and body mass explain a low proportion of the existing variance (r^2
20 653 <0.60 ; Table 4). Furthermore, the phylogenetic signal is low ($\lambda \sim 0.3$; see Table 4)
21 654 suggesting that closely related species are less likely to exhibit similar relative and
22 655 absolute petrosal lobule sizes and that other factors may affect the size of this brain
23 656 structure. The size of the petrosal lobules of *M. crusafonti* is equivalent to the value
24 657 expected for its endocranial volume compared to modern sciurids (Fig. 9E). Four extant
25 658 flying squirrels are below the regression line while the remaining three (i.e. *Pe. petaurista*,
26 659 *A. tephromelas* and *M. crusafonti*) are above it. This relationship is nearly identical when
27 660 looking at the relationship between petrosal lobule size and body mass; however, in this
28 661 instance, *M. crusafonti* lies slightly closer to *Pe. petaurista* and well above the regression
29 662 line (Fig. 9F). It is worth noting that one extant flying squirrel (*Petinomys setosus*) in our
30 663 dataset lacks the subarcuate fossa entirely (Table 3; Grau-Camats *et al.* 2022, table S4)
31 664 and therefore has no petrosal lobules on the endocast (Bertrand *et al.* 2017).

32
33
34
35
36
37
38
39
40
41
42
43
44
45
46
47
48
49 665 *Cranial nerves and blood vessels.* The ventral region of the endocast is damaged,
50 666 particularly on its posterior half, but several cranial nerves can be observed (Fig. 7B;
51 667 Appendix S1). Casts of both optic nerves and the optic chiasm are partly preserved in *M.*

1
2
3
4
5
6
7
8
9
10 668 *crusafonti*, with the chiasm being located just anterior to the point at which the
11 669 oculomotor nerve would have left the brain. Its location is difficult to identify as this area
12 670 of the cranium is not well-preserved; however, the chiasm appears to be located dorsal to
13 671 the posterior nasal spine (Fig. 7B). The sphenorbital fissure is not preserved. Casts of the
14 672 buccinator and masseteric nerves (branches of nerve V₃) are partly preserved on both
15 673 sides and exit through the masticatory foramen, which demonstrates that they would have
16 674 had a course separate from the other parts of V₃ exiting through the foramen ovale (Fig.
17 675 7). The casts of mandibular (V₃), facial (VII) and vestibulocochlear (VIII) nerves are
18 676 observable on the left side of the endocast only. The position of the different casts of the
19 677 nerves resembles the closely-related *Pe. petaurista* (Fig. 8A). The superior sagittal sinus
20 678 is demarcated (Fig. 7A), being similar in morphology to *C. wilsoni*, *Pr. cf. rachelae* (Fig.
21 679 8C–D) and most modern sciurids in our comparative sample (see Bertrand *et al.* 2017,
22 680 2018). It differs from the condition observed in ischyromyid rodents, in which the
23 681 superior sagittal sinus is less well marked (e.g. Bertrand *et al.* 2019b). The transverse and
24 682 sigmoid sinuses are visible on the left side of the endocast of *M. crusafonti* (Fig. 7C), but
25 683 the region where the inferior petrosal sinus would have passed is not preserved. The
26 684 stapedia canal for the distal section of the stapedia artery (Wible & Shelley 2020) can
27 685 be observed on the ventral region (Fig. 7B–C) and is similarly positioned compared to
28 686 sciurids and ischyromyids (Bertrand *et al.* 2017, 2018, 2019b).

687 *Brain size and encephalization quotient*

688 The endocranial volume of *M. crusafonti* (estimated doubling the volume of the
689 most complete side, see Materials and Methods) is 10.82 cm³. The encephalization
690 quotient (EQ) calculated using the equation by Pilleri *et al.* (1984) is 1.13 (Table 3; Grau-
691 Camats *et al.* 2022, table S5). This value is higher than those calculated for ischyromyids
692 (0.50 to 0.88) and very similar to those for *C. wilsoni* (1.0) and *Pr. cf. rachelae* (1.06;

1
2
3
4
5
6
7
8
9
10 693 Fig. 10A; Bertrand *et al.* 2017, 2018, 2019b). *Miopetaurista crusafonti* has an EQ below
11 694 those of extant Sciurinae, being in the lower range of variation for Callosciurinae (Fig.
12 695 10A). Log-transformed endocranial volume shows a positive and highly significant
13 696 correlation with log-transformed body mass, the latter variable explaining great part of
14 697 the existing variance ($r^2=0.89$; see Table 4). Phylogenetic signal is relatively low ($\lambda\sim 0.4$;
15 698 see Table 4) implying that closely related species may not necessarily have a similar
16 699 brain-body mass relationship, suggesting that other factors may impact relative brain size.
17 700 When assessed against body mass, the endocranial volume of *M. crusafonti* is above the
18 701 regression line for extant squirrels, below its close relative *Pe. petaurista* (Fig. 10B).

702 DISCUSSION

703 Several studies have shown that the encephalization quotient (EQ) increases with
704 time in different mammalian orders (Jerison 1973; Radinsky 1976; Gurche 1982; Silcox
705 *et al.* 2010; Orliac & Gilissen 2012; Yao *et al.* 2012; Bertrand *et al.* 2017, 2018, 2019b,
706 2021). On the other hand, a series of papers have shown that EQ also varies as a function
707 of ecology in chiropterans and rodents (Eisenberg & Wilson 1978; Harvey *et al.* 1980;
708 Mace *et al.* 1981; Roth & Thorington 1982; Meier 1983; Pilleri *et al.* 1984; Bertrand *et*
709 *al.* 2017, 2018, 2019b). These studies found that arboreality was associated with a higher
710 EQ in rodents, probably because of the requirements of foraging in a complex three-
711 dimensional environment such as found in the treetops. Recently, Bertrand *et al.* (2016b,
712 2017, 2018, 2019b, 2021) studied the endocasts of ischyromyids and early sciurids
713 (*Cedromus wilsoni* and *Protosciurus cf. rachelae*) as compared to extant aplodontids and
714 sciurids. The Oligocene *C. wilsoni* (subfamily Cedromurinae) and *Pr. cf. rachelae*
715 (subfamily Sciurinae, tribe Sciurini), both considered to be scansorial or arboreal squirrels
716 (Korth & Samuels 2015; Bhagat *et al.* 2021), had not yet reached the EQ of their extant
717 relatives. Indeed, *Cedromus* is in the upper part of the range of extant ground squirrels,

1
2
3
4
5
6
7
8
9
10 718 while *Protosciurus* is in the lower part of the range of tree squirrels. Similarly, the EQ of
11 719 *M. crusafonti* is 1.07, which is slightly below the range of variation of extant flying
12 squirrels (1.11–1.39; Fig. 10A, Table 3; Grau-Camats *et al.* 2022, table S5), yet there is
13 720 unquestionable evidence of gliding locomotion in the genus *Miopetaurista* (Casanovas-
14 721 Vilar *et al.* 2018). Accordingly, the lower EQ suggests that there were temporal trends in
15 722 this parameter within the sciurid family, as observed in other mammalian families and
16 723 orders (e.g. Jerison 1973; Radinsky 1976; Silcox *et al.* 2010; Bertrand *et al.* 2019a). In
17 724 addition, the increase in relative brain size would have occurred independently in the
18 725 Sciurini and Pteromyini, because early members of both of these Sciurinae tribes
19 726 (*Protosciurus*, *Miopetaurista*) show lower EQs than extant representatives. Considering
20 727 that two events of EQ increase occurred in closely related clades, and that the
21 728 phylogenetic signal is low for the brain-body mass regression, it can be inferred that
22 729 changes in relative brain size may relate to factors other than phylogeny, such as
23 730 ecological transitions (Bertrand *et al.* 2017, 2018, 2021).

34 732 The comparison of the endocast of *M. crusafonti* to those of extant and extinct
35 733 sciurids, as well as to the more primitive ischyromyid rodents suggests some significant
36 734 changes in brain morphology in the flying squirrel lineage. Previous studies have shown
37 735 that an increase in neocortical surface area ratio occurs in the transition from
38 736 ischyromyids to sciurids (Bertrand *et al.* 2017, 2018, 2019a). The late Oligocene fossil
39 737 Sciurini *Pr. cf. rachelae* and the middle Miocene fossil Pteromyini *M. crusafonti* both
40 738 exhibit lower neocortical surface area ratios compared to their respective extant relatives
41 739 (Fig. 9C; Grau-Camats *et al.* 2022, table S4). Therefore, neocortical surface ratio would
42 740 have increased independently in tree and flying squirrels, which is the likely cause for the
43 741 apparent independent increases in EQ discussed above. However, the independent
44 742 increase in neocortical surface area cannot be solely explained by a possible shift in

1
2
3
4
5
6
7
8
9
10 743 ecology because all extinct and extant squirrels have larger neocortices than ischyromyid
11 744 rodents. The gradual increase in neocortical surface area appears to more closely follow
12 745 a temporal trend than relative brain size and suggests that phylogeny may have more
13 746 impact on the neocortical size than on overall brain size in our sample. We note that if
14 747 Ischyromyidae are not included in the estimation of λ for the neocortex, the phylogenetic
15 748 signal for the relative size of this brain region is markedly lower (Table 4) as all extant
16 749 squirrels have a higher neocortical surface area compared to extinct squirrels.

22 750 Previous studies have shown that an increase in the absolute size of the petrosal
23 751 lobules occurred in the evolution of the sciurids from ischyromyids as a response to a
24 752 more arboreal lifestyle in the former group (Bertrand *et al.* 2017, 2018, 2019b). Our
25 753 results show a low phylogenetic signal, thus agreeing with these earlier studies, in that
26 754 factors other than shared evolutionary story have an important effect on the relative and
27 755 absolute size of the petrosal lobules. Extant pteromyins of our sample have relatively
28 756 smaller petrosal lobules compared to sciurins (Fig. 9E; Bertrand *et al.* 2017; Grau-Camats
29 757 *et al.* 2022, table S4). This difference is already apparent in Miocene taxa. Indeed, while
30 758 the tree squirrel *Pr. cf. rachelae* has relatively large petrosal lobules, the flying squirrel
31 759 *M. crusafonti* shows a lower relative size, thus resembling its extant relatives (Fig. 9E;
32 760 Grau-Camats *et al.* 2022, table S4). This suggests a decrease in the relative size of the
33 761 petrosal lobules in the evolution of flying squirrels which might be related to a packing
34 762 problem due to the constraints inherent to a skull built to be aerodynamic for gliding (see
35 763 also Bertrand *et al.* 2021). The functional elements of the petrosal lobules might still be
36 764 present but in the non-petrosal lobule part of the cerebellum. However, an alternative
37 765 explanation could be related to a specific adaptation. Tree squirrels spend a considerable
38 766 amount of time on thin and unstable branches, which implies that balance and control of
39 767 the head and eye movements are crucial for these animals. In contrast, flying squirrels

1
2
3
4
5
6
7
8
9
10 768 have a different lifestyle in the trees and to propel themselves in the air, they use more
11 769 stable and sturdy branches and trunks (Bishop 2006). This suggests that flying squirrels
12 770 might require less overall eye movement control compared to tree squirrels while
13 771 navigating the canopy. Pteromyini also have larger auditory bullae compared to tree
14 772 squirrels (Lu *et al.* 2014). These structures are in contact with the braincase and more
15 773 specifically with the subarcuate fossa. Using allometric shape deformations, Lu *et al.*
16 774 (2014) showed that the shape of different cranial regions (e.g. auditory bulla and vault-
17 775 occiput roundness) changed simultaneously from small to large squirrel specimens.
18 776 Therefore, enlarged bullae may influence and possibly reduce the space for the petrosal
19 777 lobules. Alternatively, the auditory bulla may represent a separate module, meaning that
20 778 the development of both units could be independent. Ultimately, more work will be
21 779 required to test these hypotheses. The same authors suggested that because the bullae are
22 780 so large in flying squirrels, hearing might be crucial while gliding. The parietal region of
23 781 the brain of flying squirrels appears to be more developed, which could potentially
24 782 suggest enhanced hearing (Bertrand *et al.* 2019a). Other studies have indicated that flying
25 783 squirrels, which are nocturnal gliders, might be using ultrasounds like echolocating bats
26 784 to ease navigation while gliding (Muul & Alley 1963; but see Chattin 1969). More
27 785 recently, Murrant *et al.* (2013) identified that flying squirrels were reacting to their own
28 786 high-frequency vocalizations and therefore were capable to hear ultrasonic sounds. The
29 787 use of echolocation in flying squirrels is debated and has just begun to be studied in detail,
30 788 but there is no direct evidence of echo-based navigation so far (Newar & Bowman 2020).
31 789 Flying squirrels have large eyes and undoubtedly use visual cues during glides, but they
32 790 may be also assisted by the use of ultrasound (Murrant *et al.* 2013). Therefore, the
33 791 observed decrease in the size of the petrosal lobules could result from an accommodation
34 792 for other biological needs such as hearing. More work is required to better understand the

1
2
3
4
5
6
7
8
9
10 793 relationship between the neurosensory system of flying squirrels and how they navigate
11 794 through the canopy.

12
13 795 Finally, previous studies have shown that a decrease in the size of the olfactory
14
15 796 bulbs occurred through time from ischyromyids to sciurids (Bertrand *et al.* 2017, 2018,
16
17 797 2019b). The relative size of the olfactory bulbs in *M. crusafonti* is slightly below the range
18
19 798 of to those of other members of the subtribe Pteromyina (i.e. large flying squirrel clade),
20
21 799 including the closely related *Pe. petaurista*, while that of the sciurid *Pr. cf. rachelae* is
22
23 800 conspicuously in the upper range of the extant tree squirrels variation (Grau-Camats *et al.*
24
25 801 2022, table S4). Interestingly, *Glaucomyia volans*, *Hylopetes spadiceus* and *Petinomys*
26
27 802 *setosus*, the studied members of the subtribe Glaucomyina (i.e. small flying squirrel
28
29 803 clade), all show relatively larger olfactory bulbs, in the range of other extant squirrel
30
31 804 groups (see Grau-Camats *et al.* 2022, table S4). This could suggest that a decrease in the
32
33 805 relative size of the olfactory bulbs occurred after the Pteromyina/Glaucomyina split.
34
35 806 Despite exhibiting a relatively small neocortex, closer to the condition in other Oligocene
36
37 807 squirrels rather than to extant species, *M. crusafonti* already exhibits features
38
39 808 characteristic of Pteromyini (and more specifically the Pteromyina) such as low petrosal
40
41 809 lobule and olfactory bulb volume ratios.

42 810 **CONCLUSION**

43 811 Squirrels are generally regarded as an anatomically conservative group and flying
44
45 812 squirrels are no exception, the oldest skeleton of a flying squirrel, belonging to
46
47 813 *Miopetaurista neogrivensis* and dating back to 11.6 Ma, being very similar in many
48
49 814 aspects of morphology to the extant giant flying squirrel *Petaurista* (Casanovas-Vilar *et*
50
51 815 *al.* 2018). The crania of both *M. neogrivensis* and the closely-related *Miopetaurista*
52
53 816 *crusafonti* described here are also remarkably similar to those of *Petaurista* and other
54
55 817 large flying squirrels (subtribe Pteromyina) such as *Aeromys* and *Biswamoyopterus*,

1
2
3
4
5
6
7
8
9
10 818 differing only in cheek tooth morphology and a few minor details in the cranium, such as
11 819 the morphology of the temporal ridges. Endocranial morphology, as well as the relative
12 820 volume of the different brain regions are very similar to other Pteromyina, showing for
13 821 example the relatively reduced petrosal lobules characteristic of flying squirrels in
14 822 comparison to other extant squirrels. However, the encephalization quotient (EQ) of *M.*
15 823 *crusafonti* is slightly below that of extant flying squirrels. A temporal trend in EQ increase
16 824 has been previously reported for sciurids and other mammal families (Jerison 1973;
17 825 Radinsky 1976; Gurche 1982; Silcox *et al.* 2010; Orliac & Gilissen 2012; Yao *et al.* 2012;
18 826 Bertrand *et al.* 2017, 2018, 2019b), but this parameter has also been shown to vary with
19 827 locomotor mode, arboreal and gliding rodent species showing higher values than
20 828 terrestrial ones (Bertrand *et al.* 2021). Since *Miopetaurista* was certainly a glider, like its
21 829 extant relatives, the conspicuously lower EQ must be attributed to its older age rather than
22 830 to different locomotion. Even though this should be tested in additional squirrel groups,
23 831 these results support an independent temporal increase in EQ in different squirrel clades,
24 832 further showing that, in terms of relative brain size, flying squirrels are not so
25 833 conservative.

26
27
28
29
30
31
32
33
34
35
36
37
38 834 *Author contributions.* MGC, OCB, MTS and ICV contributed to the conception and
39 835 design of the study. JP acquired the CT data, MGC, OCB, SLT segmented the specimens
40 836 and acquired quantitative measurements. MGC and OCB carried out the statistical
41 837 analyses. MGC and OCB drafted the article with important contributions by all other
42 838 authors. All authors gave final approval before submission.

43
44
45
46
47
48 839 *Acknowledgements.* This publication is part of project I+D+i PID2020-117289GBI00
49 840 funded by MCIN/AEI/10.13039/501100011033/. It has also been supported by the
50 841 Spanish Agencia Estatal de Investigación and European Regional Development Fund of
51 842 the European Union (CGL2016-76431-P and CGL2017-82654-P); the Generalitat de

1
2
3
4
5
6
7
8
9
10 843 Catalunya (CERCA Programme); a Marie Skłodowska-Curie Actions: Individual
11 844 Fellowship (H2020-MSCA-IF-2018-2020; No. 792611) to O.C.B; an NSERC Discovery
12 845 Grant to M.T.S.; and the Ministerio de Economía y Competitividad (RYC-2013-12470 to
13 846 IC-V). IC-V is member of the consolidated research group 2017 SGR 116 of the
14 847 Generalitat de Catalunya. The authors thank Sergio Llácer (ICP) for his help with
15 848 specimen segmentation, and Sergio Llácer and Javier Serrano (ICP) for preparing the
16 849 video for Appendix S1. We also thank L. W. Van den Hoek Ostende, S. Van der Mije
17 850 and P. Kaminga (Naturalis Biodiversity Center, Leiden, the Netherlands) for their
18 851 assistance during the study of the squirrel collections kept at their institution. We thank
19 852 S. Thomas for her technical comments and assistance in the preparation of tables and
20 853 figures. The constructive comments by the two reviewers of this manuscript (J. Mougoust
21 854 and M.V. Sinita) as well as by handling editor (L. Hautier) certainly helped to improve
22 855 the final result.

856 DATA ARCHIVING STATEMENT

857 Data for this study are available in the Dryad Digital Repository:
858 <https://doi.org/10.5061/dryad.5qfttdz4p>. 3D surface models of the *Miopetaurista*
859 *crusafonti* cranium and endocast SNSB 1978 V 1 from Gumpersdorf are available from
860 MorphoSource: <https://doi.org/10.17602/M2/M419287>;
861 <https://doi.org/10.17602/M2/M418084>; <https://doi.org/10.17602/M2/M418059>.

Commented [ST1]: AUTHOR: If you have not already done so, please make your MorphoSource record public (even if the files are restricted download). If you have difficulty doing this, please contact morphosource@duke.edu

863 SUPPORTING INFORMATION

864 Additional supporting information can be found in the online version of this article.

1
2
3
4
5
6
7
8
9
10 865 Appendix S1. Animated rendering of the virtual model of the cranium of *Miopetaurista*
11 866 *crusafonti* (SNSB 1978 V 1) from Gumpersdorf (Bavaria) based on μ CT
12 867 data. Main anatomical elements of the cranium and the endocast are
13 868 indicated.

14
15
16
17 869 **REFERENCES**

- 18
19
20 870 ABDUL AZIZ, H., BÖHME, M., ROCHOLL, A., PRIETO, J., WIJBRANS, J. R.,
21 871 BACHTADSE, V. and ULBIG, A. 2010. Integrated stratigraphy and $^{40}\text{Ar}/^{39}\text{Ar}$
22 872 chronology of the early to middle Miocene Upper Freshwater Molasse in western
23 873 Bavaria (Germany). *International Journal of Earth Sciences*, **99**, 1859–1886.
- 24
25
26 874 ASHER, R. J., SMITH, M. R., RANKIN, A. and EMRY, R. J. 2019. Congruence, fossils
27 875 and the evolutionary tree of rodents and lagomorphs. *Royal Society Open Science*,
28 876 **6**, 190387.
- 29
30
31
32 877 BALL, S. S. and ROTH, V. L. 1995. Jaw muscles of New World squirrels. *Journal of*
33 878 *Morphology*, **224**, 265–291.
- 34
35
36 879 BAPST, D. W. 2012. paleotree: an R package for paleontological and phylogenetic
37 880 analyses of evolution. *Methods in Ecology & Evolution*, **3**, 803–807.
- 38
39 881 BAPST, D. W. 2013. A stochastic rate-calibrated method for time-scaling phylogenies of
40 882 fossil taxa. *Methods in Ecology & Evolution*, **4**, 724–733.
- 41
42
43 883 BAPST, D. W. 2014. Preparing paleontological datasets for phylogenetic comparative
44 884 methods. 515–544. In GARAMSZEGI, L. Z. (ed.) *Modern phylogenetic*
45 885 *comparative methods and their application in evolutionary biology: Concepts and*
46 886 *practice*. Springer.
- 47
48
49 887 BERTRAND, O. C. and SILCOX, M. T. 2016. First virtual endocasts of a fossil rodent:
50 888 *Ischyromys typus* (Ischyromyidae, Oligocene) and brain evolution in rodents.
51 889 *Journal of Vertebrate Paleontology*, **36**, e1095762.

1
2
3
4
5
6
7
8
9
10
11
12
13
14
15
16
17
18
19
20
21
22
23
24
25
26
27
28
29
30
31
32
33
34
35
36
37
38
39
40
41
42
43
44
45
46
47
48
49
50
51
52
53
54
55
56
57
58
59
60

- 890 BERTRAND, O. C., SCHILLACI, M. A. and SILCOX, M. T. 2016a. Cranial dimensions
891 as estimators of body mass and locomotor habits in extant and fossil rodents.
892 *Journal of Vertebrate Paleontology*, **36**, e1014905.
- 893 BERTRAND, O. C., AMADOR-MUGHAL, F. and SILCOX, M. T. 2016b. Virtual
894 endocasts of Eocene *Paramys* (Paramyinae): oldest endocranial record for
895 Rodentia and early brain evolution in Euarchontoglires. *Proceedings of the Royal
896 Society B*, **283**, 20152316.
- 897 BERTRAND, O. C., AMADOR-MUGHAL, F. and SILCOX, M. T. 2017. Virtual
898 endocast of the early Oligocene *Cedromus wilsoni* (Cedromurinae) and brain
899 evolution in squirrels. *Journal of Anatomy*, **230**, 128–151.
- 900 BERTRAND, O. C., AMADOR-MUGHAL, F., LANG, M. M. and SILCOX, M. T. 2018.
901 Virtual endocasts of fossil Sciuroidea: brain size reduction in the evolution of
902 fossoriality. *Palaeontology*, **61**, 919–948.
- 903 BERTRAND, O. C., SAN MARTIN-FLORES, G. and SILCOX, M. T. 2019a.
904 Endocranial shape variation in the squirrel-related clade and their fossil relatives
905 using 3D geometric morphometrics: contributions of locomotion and phylogeny
906 to brain shape. *Journal of Zoology*, **308**, 197–211.
- 907 BERTRAND, O. C., AMADOR-MUGHAL, F., LANG, M. M. and SILCOX, M. T.
908 2019b. New virtual endocasts of Eocene Ischyromyidae and their relevance in
909 evaluating neurological changes occurring through time in Rodentia. *Journal of
910 Mammalian Evolution*, **26**, 345–371.
- 911 BERTRAND, O. C., SHELLEY, S. L., WIBLE, J. R., WILLIAMSON, T. E.,
912 HOLBROOK, L. T., CHESTER, S. G. B., BUTLER, I. B. and BRUSATTE, S.
913 L. 2020. Virtual endocranial and inner ear endocasts of the Paleocene ‘condylarth’

- 1
2
3
4
5
6
7
8
9
10 914 *Chriacus*: new insight into the neurosensory system and evolution of early
11 placental mammals. *Journal of Anatomy*, **236**, 21–49.
12
13 916 BERTRAND, O. C., PÜSCHEL, H. P., SCHWAB, J. A., SILCOX, M. T. and
14 BRUSATTE, S. L. 2021. The impact of locomotion on the brain evolution of
15 squirrels and close relatives. *Communications Biology*, **4**, 460.
16
17 918
18 919 BHAGAT, R., BERTRAND, O. C. and SILCOX, M. T. 2021. Evolution of arboreality
19 and fossoriality in squirrels and aplodontid rodents: Insights from the semicircular
20 canals of fossil rodents. *Journal of Anatomy*, **238**, 96–112.
21
22 921
23 922 BININDA-EMONDS, O. R. P., CARDILLO, M., JONES, K. E., MACPHEE, R. D. E.,
24 BECK, R. M. D., GRENYER, R., PRICE, S. A., VOS, R. A., GITTLEMAN, J.
25 L. and PURVIS, A. 2007. The delayed rise of present-day mammals. *Nature*, **446**,
26 507–512.
27
28 925
29 926 BISHOP, K. L. 2006. The relationship between 3-D kinematics and gliding performance
30 in the southern flying squirrel, *Glaucomys volans*. *Journal of Experimental*
31 *Biology*, **209**, 689–701.
32
33 927
34 928
35 929 BRAUER, K. and SCHOBER, W. 1970. *Katalog der Säugetiergehirne. Catalogue of*
36 *mammalian brains*. VEB Gustav Fischer, Jena, Germany.
37
38 930
39 931 DE BRUIJN, H. 1999. Superfamily Sciuroidea. 271–280. In RÖSSNER, G. E. and
40 HEISSIG, K. (eds) *The Miocene land mammals of Europe*. Friedrich Pfiel.
41
42 932
43 933 CASANOVAS-VILAR, I., ALMÉCIJA, S. and ALBA, D. M. 2015. Late Miocene flying
44 squirrels from Can Llobateres 1 (Vallès-Penedès Basin, Catalonia): systematics
45 and palaeobiogeography. *Palaeobiodiversity and Palaeoenvironments*, **95**, 353–
46 372.
47
48 935
49 936
50 937 CASANOVAS-VILAR, I., GARCIA-PORTA, J., FORTUNY, J., SANISIDRO, Ó.,
51 PRIETO, J., QUEREJETA, M., LLÁCER, S., ROBLES, J. M., BERNARDINI,
52
53 938

- 1
2
3
4
5
6
7
8
9
10 939 F. and ALBA, D. M. 2018. Oldest skeleton of a fossil flying squirrel casts new
11 940 light on the phylogeny of the group. *ELife*, **7**, e39270.
- 13 941 CHATTIN, D. 1969. Acoustical echolocation in flying squirrels. BA thesis. Reed
14 942 College, Portland, Oregon, USA, 76 pp.
- 16 943 DAAMS, R. 1977. Aragonian sciuroptera (Sciuridae, Rodentia, Mammalia) from Spain.
18 944 *Proceedings of the Koninklijke Nederlandse Akademie van Wetenschappen B*,
20 945 **80(5)**, 356–359.
- 22 946 DAXNER-HÖCK, G. and MEIN, P. 1975. Taxonomische Probleme um das Genus
23 947 *Miopetaurista* Kretzoi, 1962 (Fam. Sciuridae). *Paläontologische Zeitschrift*, **49**,
25 948 75–77.
- 27 949 DAXNER-HÖCK, G. and HÖCK, E. 2015. *Catalogus Fossilium Austriae. Ein*
28 950 *systematisches Verzeichnis aller auf österreichischem Gebiet festgestellten*
30 951 *Fossilien. Band 4. Rodentia neogenica. Catalogus Fossilium Austriae. Ein*
32 952 *Systematisches Verzeichnis Aller Auf Österreichischem Gebiet Festgestellten*
34 953 *Fossilien*. Verlag der Österreichischen Akademie der Wissenschaften.
- 36 954 EISENBERG, J. F. and WILSON, D. E. 1978. Relative brain size and feeding strategies
37 955 in the Chiroptera. *Evolution*, **32**, 740–751.
- 39 956 EMRY, R. J. and KORTH, W. W. 2007. A new genus of squirrel (Rodentia, Sciuridae)
41 957 from the mid-Cenozoic of North America. *Journal of Vertebrate Paleontology*,
43 958 **27**, 693–698.
- 45 959 FABRE, P.-H., HAUTIER, L., DIMITROV, D. and DOUZERY, E. J. P. 2012. A glimpse
46 960 on the pattern of rodent diversification: a phylogenetic approach. *BMC*
48 961 *Evolutionary Biology*, **12**, 88.
- 50 962 FAHLBUSCH, V. 1979. Flughörnchen-Schädel (*Miopetaurista crusafonti*; Inv.-Nr. 1978
51 963 V1). **7**, 18–19.

- 1
2
3
4
5
6
7
8
9
10 964 FRANZEN, J. L. and STORCH, G. 1975. Die unterpliozäne (turolische) Wirbeltierfauna
11 965 von Dorn-Dürkheim, Rheinhessen (SW-Deutschland). 1. Entdeckung, Geologie,
12 966 Mammalia: Carnivora, Proboscidea, Rodentia. Grabungsergebnisse 1972-1973.
13 967 *Senckenbergiana Lethaea*, **56**, 233–303.
- 16 968 FRANZEN, J. L., PICKFORD, M. and COSTEUR, L. 2013. Palaeobiodiversity,
17 969 palaeoecology, palaeobiogeography and biochronology of Dorn-Dürkheim 1—a
18 970 summary. *Palaeobiodiversity & Palaeoenvironments*, **93**, 277–284.
- 22 971 GRAFEN, A. and HAMILTON, W. D. 1989. The phylogenetic regression. *Philosophical*
23 972 *Transactions of the Royal Society B*, **326**, 119–157.
- 26 973 GRAU-CAMATS, M., BERTRAND, O. C., PRIETO, J., LÓPEZ-TORRES, S.,
27 974 SILCOX, M. T. and CASANOVAS-VILAR, I. 2022. Data from: A *Miopetaurista*
28 975 (*Sciuridae*, Rodentia) cranium from the middle Miocene of Bavaria (Germany)
29 976 and brain evolution in flying squirrels. *Dryad Digital Repository*.
30 977 <https://doi.org/10.5061/dryad.5qfttdz4p>
- 34 978 GREGOR, H.-J. 1982. *Die jungtertiären Floren Süddeutschlands. Paläokarpologie,*
35 979 *Phytostratigraphie, Paläoökologie, Paläoklimatologie.* Ferdinand Enke,
36 980 Stuttgart.
- 39 981 GURCHE, J. A. 1982. Early primate brain evolution. 227–246. In ARMSTRONG, E. and
40 982 FALK, D. (eds) *Primate brain evolution: Methods and concepts.* Springer.
- 43 983 HAN, G., MAO, F., BI, S., WANG, Y. and MENG, J. 2017. A Jurassic gliding
44 984 euharamiyidan mammal with an ear of five auditory bones. *Nature*, nature24483.
- 47 985 HARVEY, P. H., CLUTTON-BROCK, T. H. and MACE, G. M. 1980. Brain size and
48 986 ecology in small mammals and primates. *Proceedings of the National Academy*
49 987 *of Sciences*, **77**, 4387–4389.

- 1
2
3
4
5
6
7
8
9
10 988 HERRON, M. D., CASTOE, T. A. and PARKINSON, C. L. 2004. Sciurid phylogeny and
11 the paraphyly of Holarctic ground squirrels (*Spermophilus*). *Molecular*
12 *Phylogenetics & Evolution*, **31**, 1015–1030.
- 13
14
15 991 HILGEN, F. J., LOURENS, L. J. and VAN DAM, J. A. 2012. The Neogene Period. 923–
16 978. In GRADSTEIN, F. M., OGG, J. G., SCHMITZ, M. and OGG, G. (eds) *The*
17 *geologic time scale 2012*. Elsevier.
- 18
19
20 994 HUELSENBECK, J. P. and RONQUIST, F. 2001. MRBAYES: Bayesian inference of
21 phylogenetic trees. *Bioinformatics*, **17**, 754–755.
- 22
23
24 996 IVES, A. R. 2019. R2s for correlated data: phylogenetic models, LMMs, and GLMMs.
25 *Systematic Biology*, **68**, 234–251.
- 26
27 998 JACKSON, S. 2012. *Gliding mammals of the world*. CSIRO Publishing.
- 28
29 999 JACKSON, S. M. and THORINGTON, R. W. Jr 2012. *Gliding mammals: Taxonomy of*
30 *living and extinct species*. Smithsonian Contributions to Zoology. Smithsonian
31 Institution Scholarly Press.
- 32
33
34 1002 JERISON, H. J. 1973. *Evolution of the brain and intelligence*. Academic Press.
- 35
36 1003 JERISON, H. J. 2012. Digitized fossil brains: neocorticalization. *Biolinguistics*, **6**, 383–
37 392.
- 38
39
40 1005 KIRSCHER, U., PRIETO, J., BACHTADSE, V., AZIZ, H. A., DOPPLER, G.,
41 HAGMAIER, M. and BÖHME, M. 2016. A biochronologic tie-point for the base
42 of the Tortonian stage in European terrestrial settings: Magnetostratigraphy of the
43 topmost Upper Freshwater Molasse sediments of the North Alpine Foreland Basin
44 in Bavaria (Germany). *Newsletters on Stratigraphy*, **49**, 445–467.
- 45
46
47 1009 KORTH, W. W. 1994. *The Tertiary record of rodents in North America*. Plenum Press.
- 48
49 1010 KORTH, W. W. and EMRY, R. J. 1991. The skull of *Cedromus* and a review of the
50 *Cedromurinae* (Rodentia, Sciuridae). *Journal of Paleontology*, **65**, 984–994.
- 51
52
53
54
55
56
57
58
59
60

- 1
2
3
4
5
6
7
8
9
10 1013 KORTH, W. W. and SAMUELS, J. X. 2015. New rodent material from the John Day
11 1014 Formation (Arikareean, Middle Oligocene to Early Miocene) of Oregon. *Annals*
12 1015 *of Carnegie Museum*, **83**, 19–84.
- 15 1016 LI, Q., LI, X.-Y., JACKSON, S. M., LI, F., JIANG, M., ZHAO, W., SONG, W.-Y. and
16 1017 JIANG, X.-L. 2019. Discovery and description of a mysterious Asian flying
17 1018 squirrel (Rodentia, Sciuridae, *Biswamoyopterus*) from Mount Gaoligong,
19 1019 southwest China. *ZooKeys*, **864**, 147–160.
- 22 1020 LONG, A., BLOCH, J. I. and SILCOX, M. T. 2015. Quantification of neocortical ratios
23 1021 in stem primates. *American Journal of Physical Anthropology*, **157**, 363–373.
- 25 1022 LU, X., GE, D., XIA, L., HUANG, C. and YANG, Q. 2014. Geometric morphometric
26 1023 study of the skull shape diversification in Sciuridae (Mammalia, Rodentia).
27 1024 *Integrative Zoology*, **9**, 231–245.
- 31 1025 LUO, Z.-X., MENG, Q.-J., GROSSNICKLE, D. M., LIU, D., NEANDER, A. I.,
32 1026 ZHANG, Y.-G. and JI, Q. 2017. New evidence for mammaliaform ear evolution
33 1027 and feeding adaptation in a Jurassic ecosystem. *Nature*, **548**, 326–329.
- 36 1028 MACE, G. M., HARVEY, P. H. and CLUTTON-BROCK, T. H. 1981. Brain size and
37 1029 ecology in small mammals. *Journal of Zoology*, **193**, 333–354.
- 40 1030 MACRINI, T. E., ROUGIER, G. W. and ROWE, T. 2007. Description of a cranial
41 1031 endocast from the fossil mammal *Vincelestes neuquenianus* (Theriiformes) and
42 1032 its relevance to the evolution of endocranial characters in therians. *The*
43 1033 *Anatomical Record*, **290**, 875–892.
- 46 1034 MARTIN, R. D. 1990. *Primate origins and evolution: A phylogenetic reconstruction*.
47 1035 Princeton University Press.

- 1
2
3
4
5
6
7
8
9
10 1036 MAYR, H. 1979. Gebissmorphologische Untersuchungen an miozänen Gliriden
11 1037 Mammalia, Rodentia Süddeutschlands. PhD thesis. Ludwig-Maximilians-
12 1038 Universität München, Germany, 380 pp.
13
14
15 1039 McKENNA, M. C. and BELL, S. K. 1997. *Classification of mammals*. Columbia
16 1040 University Press.
17
18 1041 MEIER, P. T. 1983. Relative brain size within the North American Sciuridae. *Journal of*
19 1042 *Mammalogy*, **64**, 642–647.
20
21
22 1043 MEIN, P. 1970. Les sciuroptères (Mammalia, Rodentia) néogènes d'Europe Occidentale.
23 1044 *Geobios*, **3**, 7–77.
24
25 1045 MEIN, P. and ROMAGGI, J.-P. 1991. Un gliridé (mammalia, rodentia) planeur dans le
26 1046 miocène supérieur de l'Ardèche: Une adaptation non retrouvée dans la nature
27 1047 actuelle. *Geobios*, **24**, 45–50.
28
29
30 1048 MENG, J., HU, Y. and LI, C. 2003. The osteology of *Rhombomylus* (Mammalia, Glires):
31 1049 implications for phylogeny and evolution of Glires. *Bulletin of the American*
32 1050 *Museum of Natural History*, **275**, 1–247.
33
34
35 1051 MENG, J., HU, Y., WANG, Y., WANG, X. and LI, C. 2006. A Mesozoic gliding
36 1052 mammal from northeastern China. *Nature*, **444**, 889–893.
37
38
39 1053 MERCER, J. M. and ROTH, V. L. 2003. The effects of Cenozoic global change on
40 1054 squirrel phylogeny. *Science*, **299**, 1568–1572.
41
42
43 1055 MURPHY, W. J., FOLEY, N. M., BREDEMAYER, K. R., GATESY, J. and SPRINGER,
44 1056 M. S. 2021. Phylogenomics and the genetic architecture of the placental mammal
45 1057 radiation. *Annual Review of Animal Biosciences*, **9**, 29–53.
46
47
48 1058 MURRANT, M. N., BOWMAN, J., GARROWAY, C. J., PRINZEN, B., MAYBERRY,
49 1059 H. and FAURE, P. A. 2013. Ultrasonic vocalizations emitted by flying squirrels.
50 1060 *PLoS One*, **8**, e73045.
51
52
53
54
55
56
57
58
59
60

- 1
2
3
4
5
6
7
8
9
10 1061 MUUL, I. and ALLEY, J. W. 1963. Night gliders of the woodlands: vociferous
11 1062 *Glaucomys* rarely appears. *Natural History Magazine*, 72(5), 18–25.
12
13 1063 NEWAR, S. L. and BOWMAN, J. 2020. Think before they squeak: vocalizations of the
14 1064 squirrel family. *Frontiers in Ecology & Evolution*, **8**, 193.
15
16 1065 NICOLAS, V., WENDELEN, W., BARRIERE, P., DUDU, A. and COLYN, M. 2008.
17 1066 Morphometric variation in *Hylomyscus alleni* and *H. stella* (Rodentia: Muridae),
18 1067 and description of a new species. *Journal of Mammalogy*, **89**, 222–231.
19
20 1068 O’LEARY, M. A., BLOCH, J. I., FLYNN, J. J., GAUDIN, T. J., GIALLOMBARDO,
21 1069 A., GIANNINI, N. P., GOLDBERG, S. L., KRAATZ, B. P., LUO, Z.-X., MENG,
22 1070 J., NI, X., NOVACEK, M. J., PERINI, F. A., RANDALL, Z. S., ROUGIER, G.
23 1071 W., SARGIS, E. J., SILCOX, M. T., SIMMONS, N. B., SPAULDING, M.,
24 1072 VELAZCO, P. M., WEKSLER, M., WIBLE, J. R. and CIRRANELLO, A. L.
25 1073 2013. The placental mammal ancestor and the post–K–Pg radiation of placentals.
26 1074 *Science*, **339**, 662–667.
27
28 1075 ORLIAC, M. J. and GILISSEN, E. 2012. Virtual endocranial cast of earliest Eocene
29 1076 *Diacodexis* (Artiodactyla, Mammalia) and morphological diversity of early
30 1077 artiodactyl brains. *Proceedings of the Royal Society B*, **279**, 3670–3677.
31
32 1078 PAGEL, M. 1999. Inferring the historical patterns of biological evolution. *Nature*, **401**,
33 1079 877–884.
34
35 1080 PILLERI, G., GIHR, M. and KRAUS, C. 1984. Cephalization in rodents with particular
36 1081 reference to the Canadian beaver (*Castor canadensis*). 11–102. In PILLERI, G.
37 1082 (ed.) *Investigations on beavers*, Brain Anatomy Institute, Berne.
38
39 1083 PINHEIRO, J., BATES, D., DEBROY, S., SARKAR, D. and R CORE TEAM. 2020.
40 1084 *nlme: Linear and Nonlinear Mixed Effects Models*. R package. [https://cran.r-](https://cran.r-project.org/web/packages/nlme/index.html)
41 1085 [project.org/web/packages/nlme/index.html](https://cran.r-project.org/web/packages/nlme/index.html)

- 1
2
3
4
5
6
7
8
9
10 1086 PRIETO, J. and RUMMEL, M. 2016. Some considerations on small mammal evolution
11 1087 in Southern Germany, with emphasis on Late Burdigalian-Earliest Tortonian
12 1088 (Miocene) cricetid rodents. *Comptes Rendus Palevol*, **15**, 837–854.
- 15 1089 R CORE TEAM. 2020. *R: A language and environment for statistical computing*. R
16 1090 Foundation for Statistical Computing, Vienna. <https://www.R-project.org>
- 18 1091 RADINSKY, L. 1976. Oldest horse brains: more advanced than previously realized.
19 1092 *Science*, **194**, 626–627.
- 22 1093 RONQUIST, F. and HUELSENBECK, J. P. 2003. MrBayes 3: Bayesian phylogenetic
23 1094 inference under mixed models. *Bioinformatics*, **19**, 1572–1574.
- 25 1095 ROTH, V. L. and THORINGTON, R. W. Jr 1982. Relative brain size among African
26 1096 squirrels. *Journal of Mammalogy*, **63**, 168–173.
- 29 1097 SILCOX, M. T., BENHAM, A. E. and BLOCH, J. I. 2010. Endocasts of *Microsyops*
30 1098 (Microsyopidae, Primates) and the evolution of the brain in primitive primates.
31 1099 *Journal of Human Evolution*, **58**, 505–521.
- 34 1100 SIMPSON, G. G. 1945. The principles of classification and a classification of mammals.
35 1101 *Bulletin of the American Museum of Natural History*, **85**, 1–350.
- 38 1102 SINITSA, M. V., POGODINA, N. V. and KRYUCHKOVA, L. Y. 2019. The skull of
39 1103 *Spermophilus nogaici* (Rodentia: Sciuridae: Xerinae) and the affinities of the
40 1104 earliest Old World ground squirrels. *Zoological Journal of the Linnean Society*,
41 1105 **186**, 826–864.
- 45 1106 SPRINGER, M. S., MURPHY, W. J., EIZIRIK, E. and O'BRIEN, S. J. 2003. Placental
46 1107 mammal diversification and the Cretaceous–Tertiary boundary. *Proceedings of*
47 1108 *the National Academy of Sciences*, **100**, 1056–1061.

- 1
2
3
4
5
6
7
8
9
10 1109 STEPPAN, S. J., STORZ, B. L. and HOFFMANN, R. S. 2004. Nuclear DNA phylogeny
11 of the squirrels (Mammalia: Rodentia) and the evolution of arboreality from c-
12 myc and RAG1. *Molecular Phylogenetics and Evolution*, **30**, 703–719.
13
14 1111
15 1112 STORCH, G., ENGESESSER, B. and WUTTKE, M. 1996. Oldest fossil record of gliding
16 in rodents. *Nature*, **379**, 439–441.
17
18 1114 SYMONDS, M. R. E. and BLOMBERG, S. P. 2014. A Primer on Phylogenetic
19 Generalised Least Squares. In GARAMSZEGI, L. Z. (ed.) *Modern Phylogenetic*
20 *Comparative Methods and Their Application in Evolutionary Biology: Concepts*
21 *and Practice*, Springer, Berlin, Heidelberg, 105–130 pp.
22
23 1117
24 1118 THORINGTON, R. W. Jr 1984. Flying squirrels are monophyletic. *Science*, **225**, 1048–
25 1050.
26
27 1119
28 1120 THORINGTON, R. W. Jr and DARROW, K. 2000. Anatomy of the squirrel wrist: bones,
29 ligaments and muscles. *Journal of Morphology*, **246**, 85–102.
30
31 1121
32 1122 THORINGTON, R. W. Jr, PITASSY, D. and JANSA, S. A. 2002. Phylogenies of flying
33 squirrels (Pteromyinae). *Journal of Mammalian Evolution*, **9**, 99–135.
34
35 1123
36 1124 THORINGTON, R. W. Jr, SCHENNUM, C. E., PAPPAS, L. A. and PITASSY, D. 2005.
37 The difficulties of identifying flying squirrels (Sciuridae: Pteromyini) in the fossil
38 record. *Journal of Vertebrate Paleontology*, **25**, 950–961.
39
40 1126
41 1127 WAHLERT, J. H. 1985. Cranial foramina of rodents. 311–332. In LUCKETT, W. P. and
42 HARTENBERGER, J.-L. (eds) *Evolutionary relationships among rodents*,
43 Springer.
44
45 1129
46 1130 WAHLERT, J. H. 2000. Morphology of the auditory region in *Paramys copei* and other
47 Eocene rodents from North America. *American Museum Novitates*, **3307**, 1–16.
48
49 1131
50 1132 WIBLE, J. R. 1984. The ontogeny and phylogeny of the mammalian cranial arterial
51 pattern. PhD thesis. Duke University, Durham, North Carolina, USA, 705 pp.
52
53 1133
54
55
56
57
58
59
60

1
2
3
4
5
6
7
8
9
10
11
12
13
14
15
16
17
18
19
20
21
22
23
24
25
26
27
28
29
30
31
32
33
34
35
36
37
38
39
40
41
42
43
44
45
46
47
48
49
50
51
52
53
54
55
56
57
58
59
60

- 1134 WIBLE, J. R. 2008. On the cranial osteology of the Hispaniolan solenodon, *Solenodon*
1135 *paradoxus* Brandt, 1833 (Mammalia, Lipotyphla, Solenodontidae). *Annals of*
1136 *Carnegie Museum*, **77**, 321–402.
- 1137 WIBLE, J. R. and SHELLEY, S. L. 2020. Anatomy of the petrosal and middle ear of the
1138 brown rat, *Rattus norvegicus* (Berkenhout, 1769) (Rodentia, Muridae). *Annals of*
1139 *Carnegie Museum*, **86**, 1–35.
- 1140 YAO, L., BROWN, J.-P., STAMPANONI, M., MARONE, F., ISLER, K. and MARTIN,
1141 R. D. 2012. Evolutionary change in the brain size of bats. *Brain, Behavior &*
1142 *Evolution*, **80**, 15–25.
- 1143
- 1144

1145 **FIGURE CAPTIONS**

1146 **FIG. 1.** Phylogenetic relationships and age for Sciuridae and Ischyromyidae discussed in
1147 the text. Within the Sciurinae, the flying (Pteromyini) and tree squirrel (Sciurini) clades
1148 are highlighted and *Miopetaurista crusafonti* is indicated in bold. Tree topology is mostly
1149 based in Korth & Emry (1991), Meng *et al.* (2003) and Casanovas-Vilar *et al.* (2018) (see
1150 text for details). This tree is used to perform the phylogenetic generalised least squares
1151 (PGLS) analyses (see text for details).

1152 **FIG. 2.** Virtual endocast of *Miopetaurista crusafonti* (SNSB 1978 V 1) inside the
1153 translucent cranium in: A, dorsal; B, ventral; C, left lateral; D, right lateral view. Scale
1154 bar represents 10 mm. See Appendix S1 for an animated rendering of the specimen.

1155 **FIG. 3.** Cranium of *Miopetaurista crusafonti* (SNSB 1978 V 1) in: A, dorsal; B, ventral;
1156 C, left lateral; D, right lateral view. E, detail of the upper left cheek teeth in occlusal view.
1157 Scale bars represent: 10 mm (A–D); 5 mm (E). Cheek teeth measurements and
1158 comparisons are given in Table 1 and Grau-Camats *et al.* (2022, table S1), respectively;
1159 cranial measurements and comparisons are given in Table 2.

1160 **FIG. 4.** Three-dimensional model of the cranium of *Miopetaurista crusafonti* (SNSB 1978
1161 V 1) based on μ CT data and schematic drawing indicating the different anatomical
1162 elements in: A, ventral; B dorsal view. Grey shading indicates broken areas. Scale bar
1163 represents 10 mm. See Appendix S1 for an animated rendering of the specimen.

1164 **FIG. 5.** Three-dimensional model of the cranium of *Miopetaurista crusafonti* (SNSB 1978
1165 V 1) based on μ CT data and schematic drawings indicating the different anatomical
1166 elements. A, left lateral view. B, left petrosal in medial view. Grey shading indicates
1167 broken areas. Dashed lines indicate the approximate situation of anatomical features that

1
2
3
4
5
6
7
8
9
10 1168 cannot be appreciated in this view. Scale bars represent 10 mm. See Appendix S1 for an
11 1169 animated rendering of the specimen.

12
13
14 1170 **FIG. 6.** Crania of extinct and extant flying squirrels in dorsal, ventral and lateral view. A,
15 1171 *Miopetaurista crusafonti* (SNSB 1978 V 1). B, *Miopetaurista neogriviensis* (virtual
16 1172 reconstruction based on IPS56468h and IPS88677). C, *Petaurista petaurista* (ZMA
17 1173 13418). D, *Aeromys tephromelas* (RMNH 24076). E, *Petinomys sagitta* (RMNH 15512).
18 1174 Scale bars represent 10 mm. Cranial measurements and comparisons are given in Table
19 1175 2.

20
21
22
23
24
25 1176 **FIG. 7.** Endocranial morphology of the Miocene fossil flying squirrel *Miopetaurista*
26 1177 *crusafonti* (SNSB 1978 V 1). Virtual endocast of *M. crusafonti* in: A, dorsal; B, ventral;
27 1178 C, left lateral view. Scale bar represents 10 mm. See Appendix S1 for an animated
28 1179 rendering of the endocast.

29
30
31
32
33 1180 **FIG. 8.** Endocasts of various extinct and extant rodents in dorsal, ventral and right lateral
34 1181 views. A, *Petaurista petaurista* (USNM 589079). B, *Glaucomys volans* (AMNH 240290).
35 1182 C, *Cedromus wilsoni* (USNM 256584). D, *Protosciurus cf. rachelae* (YPM 14737). E,
36 1183 *Paramys delicatus* (AMNH 12506). Scale bars represent 10 mm.

37
38
39
40
41 1184 **FIG. 9.** Bivariate plots and boxplots for endocast measurements in Ischyromyidae and
42 1185 extant and extinct Sciuridae. A, bivariate plot of log₁₀ (olfactory bulb volume) versus
43 1186 log₁₀ (endocranial volume). B, bivariate plot of log₁₀ (olfactory bulb volume) versus
44 1187 log₁₀ (body mass). C, boxplot of neocortical surface area ratio. D, bivariate plot of log
45 1188 10 (neocortical surface area) versus log₁₀ (endocranial surface area). E, bivariate plot of
46 1189 log₁₀ (petrosal lobule volume) versus log₁₀ (endocranial volume). F, bivariate plot of
47 1190 log₁₀ (petrosal lobule volume) versus log₁₀ (body mass). Phylogenetic generalized
48 1191 least-square (PGLS) regression lines are included for extant Sciuridae. The position of

1
2
3
4
5
6
7
8
9
10 1192 *Miopetaurista crusafonti* SNSB 1978 V 1 from Gumpersdorf as well as that of the extant
11 1193 *Petaurista petaurista* (thick arrow) is indicated in A–B and D–F. PGLS regression results
12 1194 are given in Table 4. Residuals associated with the different PGLS regressions are given
13 1195 in Grau-Camats *et al.* (2022, table S6). Body mass, olfactory bulb, petrosal lobule and
14 1196 endocast volume (in mm³) and neocortical surface area for *Miopetaurista crusafonti* and
15 1197 other extinct and extant sciurid and ischyromyid rodents are given in Grau-Camats *et al.*
16 1198 (2022, table S4).

17 1199 **FIG. 10.** Relationship between endocranial volume and body mass and encephalization
18 1200 quotients for extinct and extant Sciuridae and Ischyromyidae (see Table 1). A, boxplot of
19 1201 EQs based on the equation by Pilleri *et al.* (1984). B, bivariate plot of log 10 (endocranial
20 1202 volume) versus log 10 (body mass) for Sciuridae and Ischyromyidae. Phylogenetic
21 1203 generalized least-square (PGLS) regression line is included for extant Sciuridae. The
22 1204 position of *Miopetaurista crusafonti* SNSB 1978 V 1 from Gumpersdorf, as well as that
23 1205 of the extant *Petaurista petaurista* (thick arrow) is indicated in B. PGLS regression results
24 1206 are given in Table 4. Residuals associated with the different PGLS regressions are given
25 1207 in Grau-Camats *et al.* (2022, table S7). Body mass and endocast volume (in mm³) for
26 1208 *Miopetaurista crusafonti* and other extinct and extant sciurid and ischyromyid rodents are
27 1209 given in Grau-Camats *et al.* (2022, table S4).

28 1210 **TABLE 1.** Cheek tooth measurements for *Miopetaurista crusafonti* 1978 V 1 from
29 1211 Gumpersdorf.

30 1212 <footnote>l, left side; r, right side. All measurements in mm.</footnote>

31 1213 **TABLE 2.** Cranial measurements for extinct and extant flying squirrels as compared to
32 1214 *Miopetaurista crusafonti* 1978 V 1 from Gumpersdorf and other extant and extinct flying
33 1215 squirrels.

1
2
3
4
5
6
7
8
9
10 1216 <footnote>Cranial measurements for the virtually reconstructed skull of *M. neogrivensis*
11 1217 are after Casanovas-Vilar *et al.* (2018). Acronyms and definitions of the measurements
12 1218 follow Nicolas *et al.* (2008) and Bertrand *et al.* (2016a): BNAS, maximum breadth of the
13 1219 nasals; BRCA, maximum breadth of the braincase; BULL, maximum length of the
14 1220 auditory bulla; CTL, length of the upper cheek tooth row; DIA, length of the diastema
15 1221 (from the alveolus of the incisor to the alveolus of the P3); HEBA, henselion–basion
16 1222 length; HEPA, henselion–palation length; IF, length of the incisive foramen; INTE,
17 1223 smallest interorbital breadth; LNAS, maximum length of the nasals; PALA, smallest
18 1224 palatal breadth; RB, maximum rostrum breadth; RH, mediosagittal projection of rostrum
19 1225 height at the anterior border of the M1; SL, maximum length of the skull. All
20 1226 measurements are in mm. Estimated measurements (due to breakage or distortion) are
21 1227 given in parentheses; ‘>’ indicates that the measurement could not be reliably taken but
22 1228 certainly exceeded the reported value.</footnote>

23
24
25
26
27
28
29
30
31
32
33 1229 **TABLE 3.** Endocranial volume, olfactory bulb, petrosal lobules, neocortical ratios and
34 1230 encephalization quotients for *Miopetaurista crusafronti* and published extant Pteromyini
35 1231 (Bertrand *et al.* 2017).

36
37
38
39 1232 <footnote>We used the formula $NS1 \times 2 / TS$ to calculate the neocortical surface area ratio.
40 1233 Volume and surface area ratios are expressed as percentages. Encephalization quotients
41 1234 were calculated using the equations of Eisenberg (1981) and Pilleri *et al.*
42 1235 (1984).</footnote>

43
44
45
46
47 1236 **TABLE 4.** Phylogenetic generalized least-square linear regressions (PGLS) for endocranial
48 1237 measurements and for total endocranial volume vs body size in our sample (see Figs 9,
49 1238 10).

1
2
3
4
5
6
7
8
9
10 1239 <footnote>For each regression, the values for the intercept, slope and associated
11 1240 significance, Pagel's λ , the pooled estimate of the residual standard error (RSE), degrees
12 1241 of freedom (df) for the model and residuals, 95 % confidence intervals for the slope (CI),
13 1242 and correlation coefficient (R^2) obtained from predicted and residual values. Residuals
14 1243 associated with the different regressions are provided in Grau-Camats *et al.* (2022, tables
15 1244 S6–S7). Body mass, olfactory bulb, petrosal lobule and endocast volume (in mm³) as well
16 1245 as neocortical surface area for *Miopetaurista crusafonti* and other extinct and extant
17 1246 sciurid and ischyromyid rodents are given in Grau-Camats *et al.* (2022, table
18 1247 S4).</footnote>

1
2
3
4
5
6
7
8
9
10
11
12
13
14
15
16
17
18
19
20
21
22
23
24
25
26
27
28
29
30
31
32
33
34
35
36
37
38
39
40
41
42
43
44
45
46
47
48
49
50
51
52
53
54
55
56
57
58
59
60

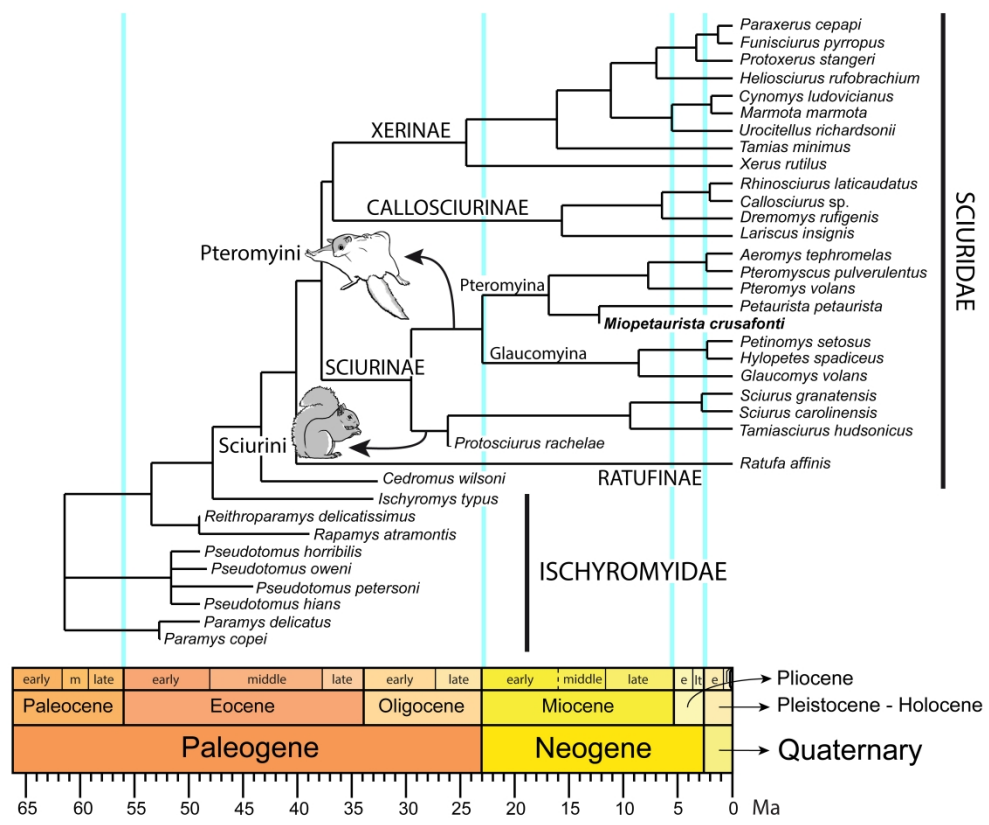


Fig. 1. Phylogenetic relationships and age for Sciuridae and Ischyromyidae discussed in the text. Within the Sciurinae, the flying (Pteromyini) and tree squirrel (Sciurini) clades are highlighted and *Miopetaurista crusafonti* is indicated in bold. Tree topology is mostly based in Korth & Emry (1991), Meng et al. (2003) and Casanovas-Vilar et al. (2018) (see text for details). This tree is used to perform the Phylogenetic Generalised Least Squares (PGLS) analyses (see text for details).

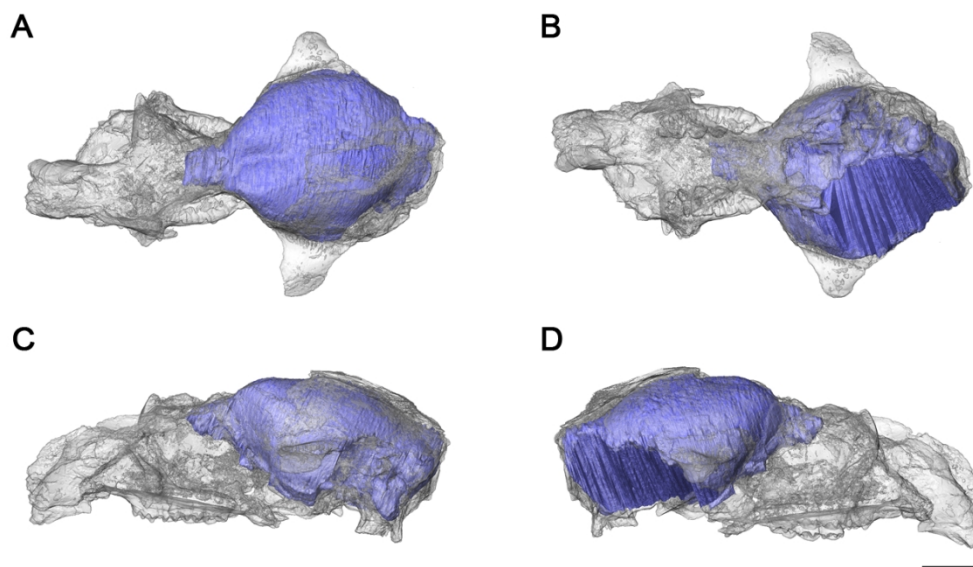


Fig. 2. Virtual endocast of *Miopetaurista crusafonti* (SNSB 1978 V 1) inside the translucent cranium in: A, dorsal; B, ventral; C, left lateral; D, right lateral view. Scale bar is 10 mm. See Appendix S1 for an animated rendering of the specimen.

109x64mm (300 x 300 DPI)

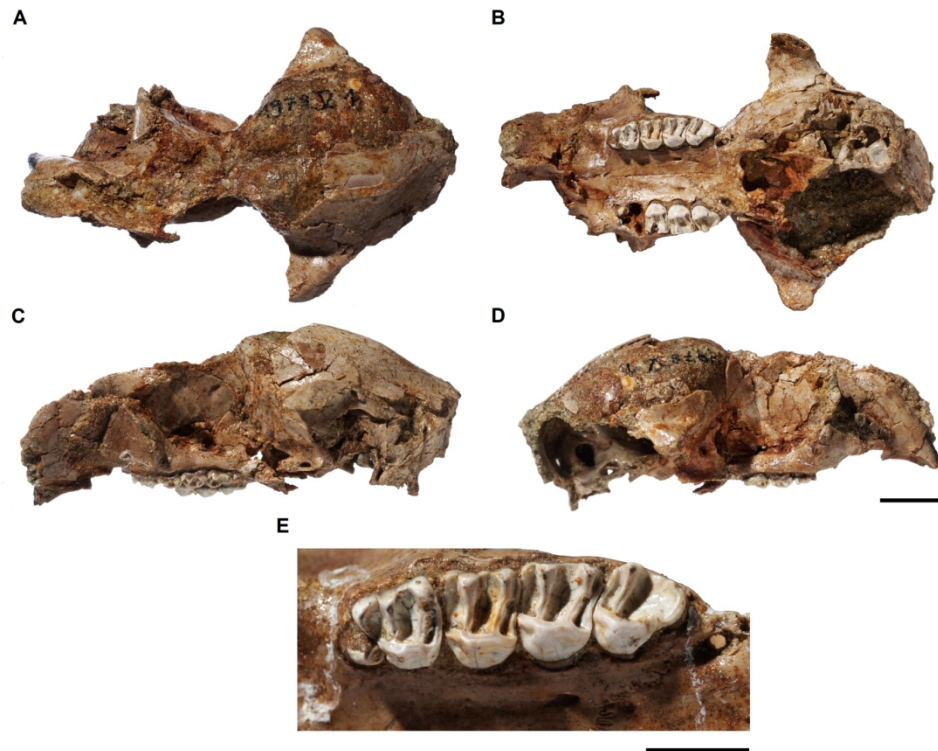


Fig. 3. Cranium of *Miopetaurista crusafonti* (SNSB 1978 V 1) in: A, dorsal; B, ventral; C, left lateral; D, right lateral view. E, detail of the upper left cheek teeth in occlusal view. Scale bar is 10 mm in figures A–D and 5 mm in figure E. Cheek teeth measurements and comparisons are given in Table 1 and Grau-Camats et al. (2021, table S1), respectively, while cranial measurements and comparisons are given in Table 2. See Appendix S1 for an animated rendering of the specimen.

166x130mm (300 x 300 DPI)

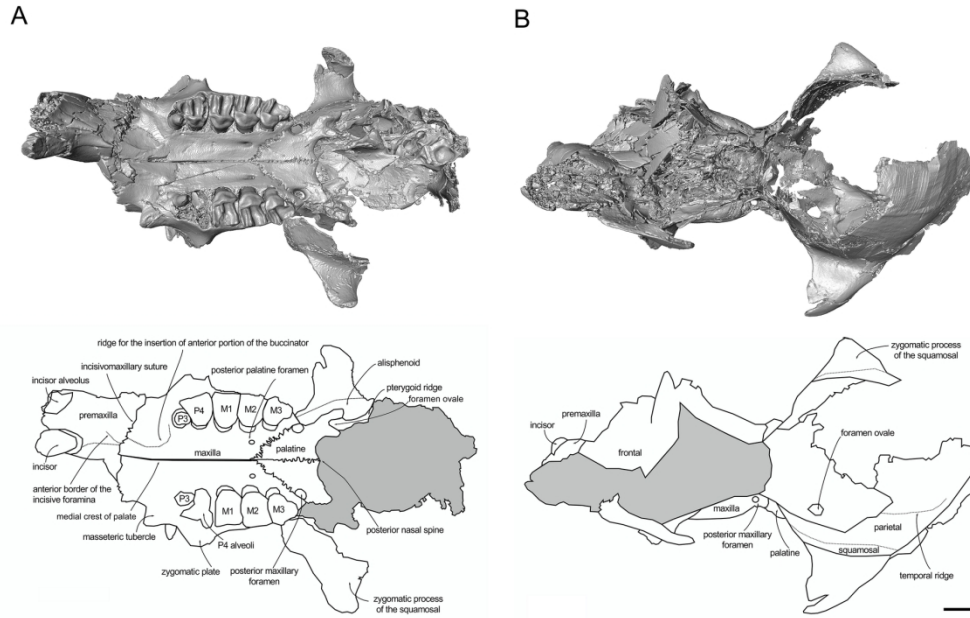
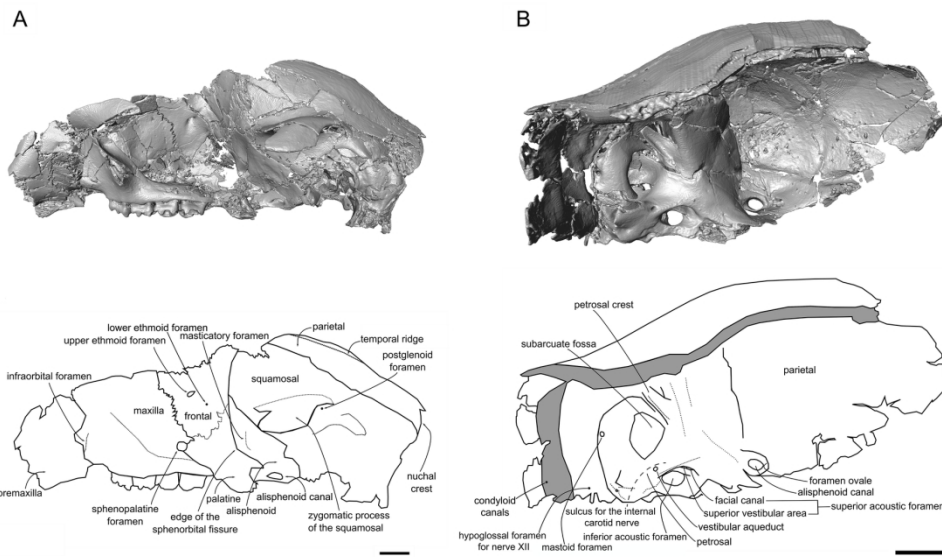


Fig. 4. Three-dimensional model of the cranium of *Miopetaurista crusafonti* (SNSB 1978 V 1) based on μ CT data and schematic drawing indicating the different anatomical elements in: A, ventral view; B dorsal view. Gray shading indicates broken areas. Scale bar is 10 mm. See Appendix S1 for an animated rendering of the specimen.

165x104mm (300 x 300 DPI)



26 Fig. 5. Three-dimensional model of the cranium of *Miopetaurista crusafonti* (SNSB 1978 V 1) based on μ CT
27 data and schematic drawing indicating the different anatomical elements in: A, left lateral view; B, left
28 petrosal in medial view. Gray shading indicates broken areas. Dashed lines indicate the approximate
29 situation of anatomical features that cannot be appreciated in this view. Scale bar is 10 mm. See Appendix
30 S1 for an animated rendering of the specimen.

31 165x97mm (300 x 300 DPI)

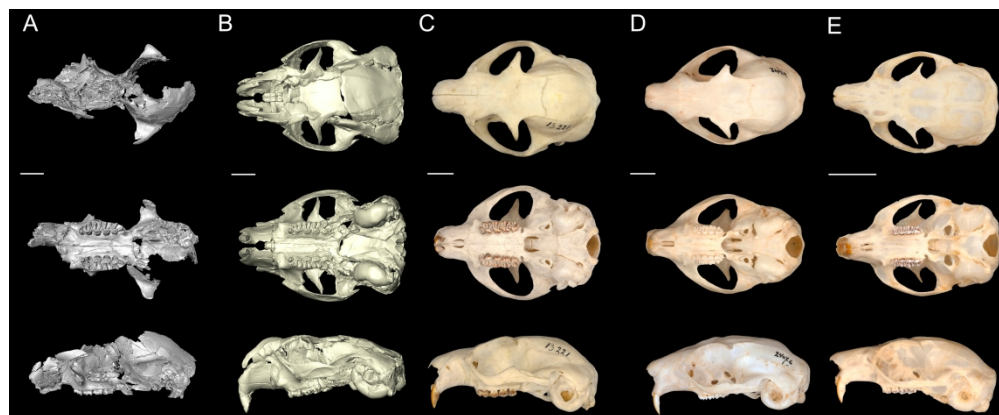


Fig. 6. Crania of extinct and extant flying squirrels in dorsal, ventral and lateral views. A, *Miopetaurista crusafonti* (SNSB 1978 V 1); B, *Miopetaurista neogriviensis* (virtual reconstruction based on IPS56468h and IPS88677); C, *Petaurista petaurista* (ZMA 13418); D, *Aeromys tephromelas* (RMNH 24076); E, *Petinomys sagitta* (RMNH 15512). Scale bars are 10 mm. Cranial measurements and comparisons are given in Table 2.

403x165mm (300 x 300 DPI)

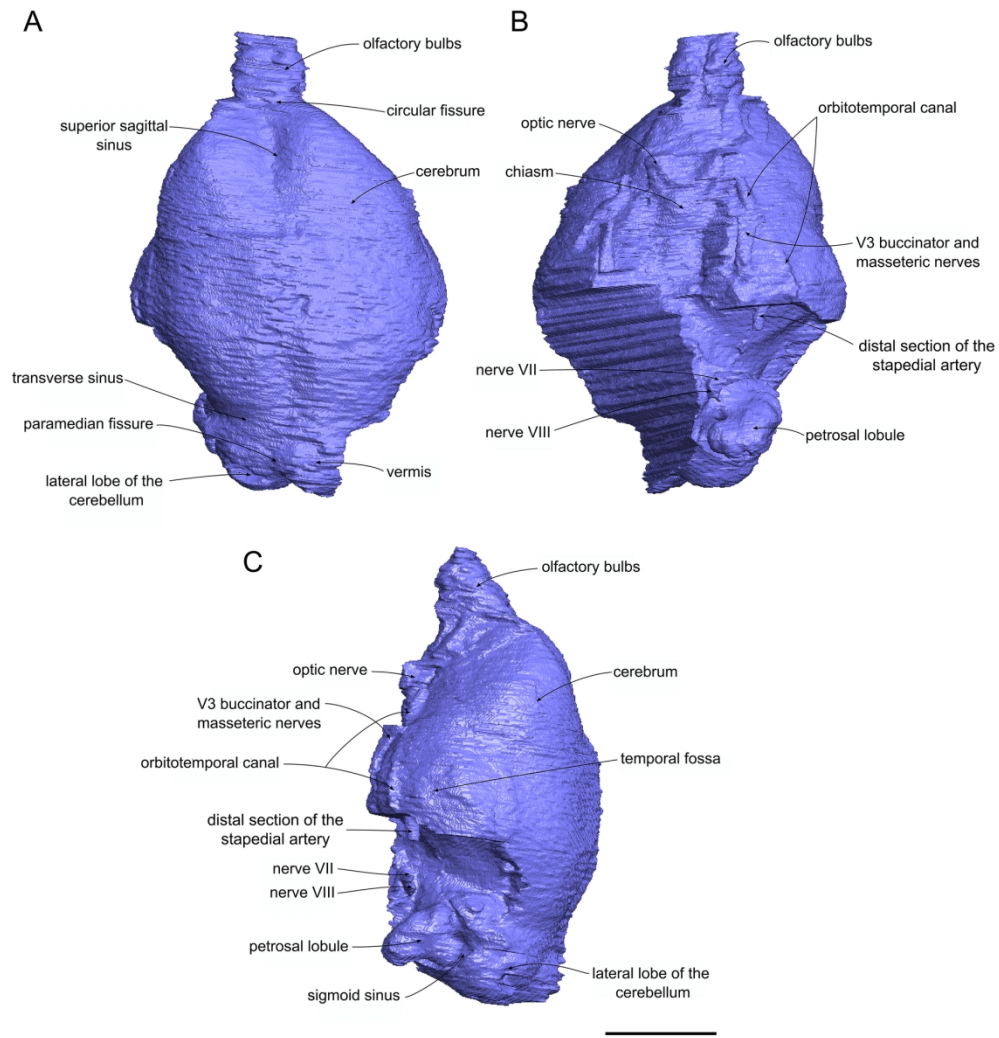


Fig. 7. Endocranial morphology of the Miocene fossil flying squirrel *Miopetaurista crusafonti* (SNSB 1978 V 1). Virtual endocast of *M. crusafonti* in: A, dorsal; B, ventral; C, left lateral view. Scale bar is 10 mm. See Appendix S1 for an animated rendering of the endocast.

165x177mm (300 x 300 DPI)

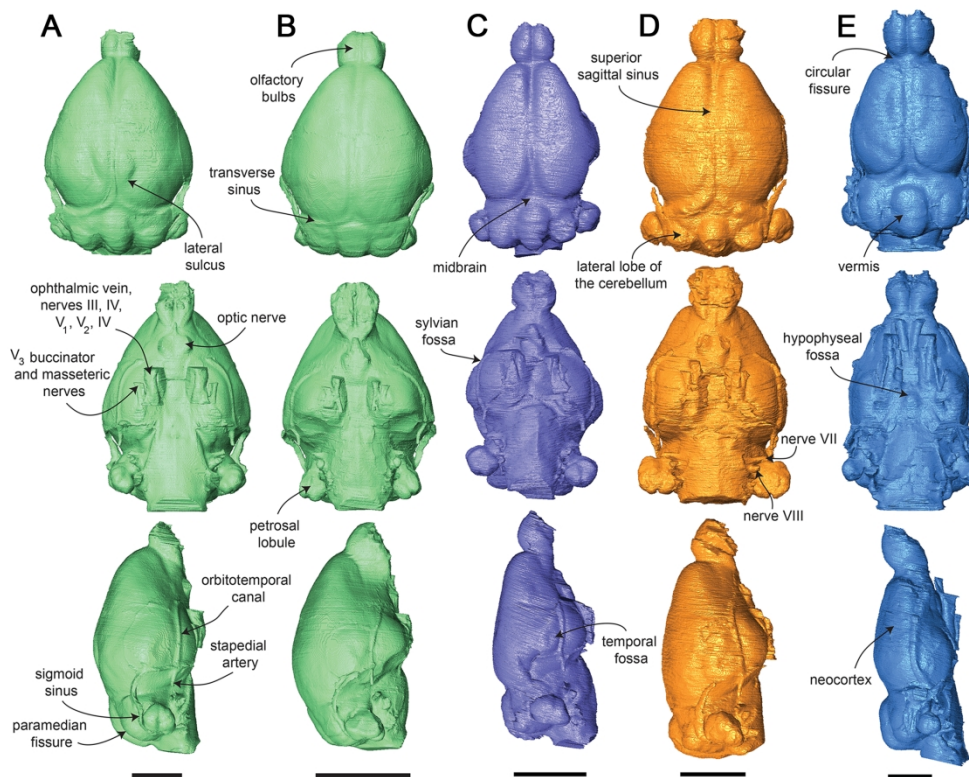


Fig. 8. Endocasts of various extinct and extant rodents in dorsal, ventral and right lateral views. A, *Petaurista petaurista* (USNM 589079); B, *Glaucomys volans* (AMNH 240290); C, *Cedromus wilsoni* (USNM 256584); D, *Protosciurus cf. rachelae* (YPM 14737); E, *Paramys delicatus* (AMNH 12506). Scale bars are 10 mm.

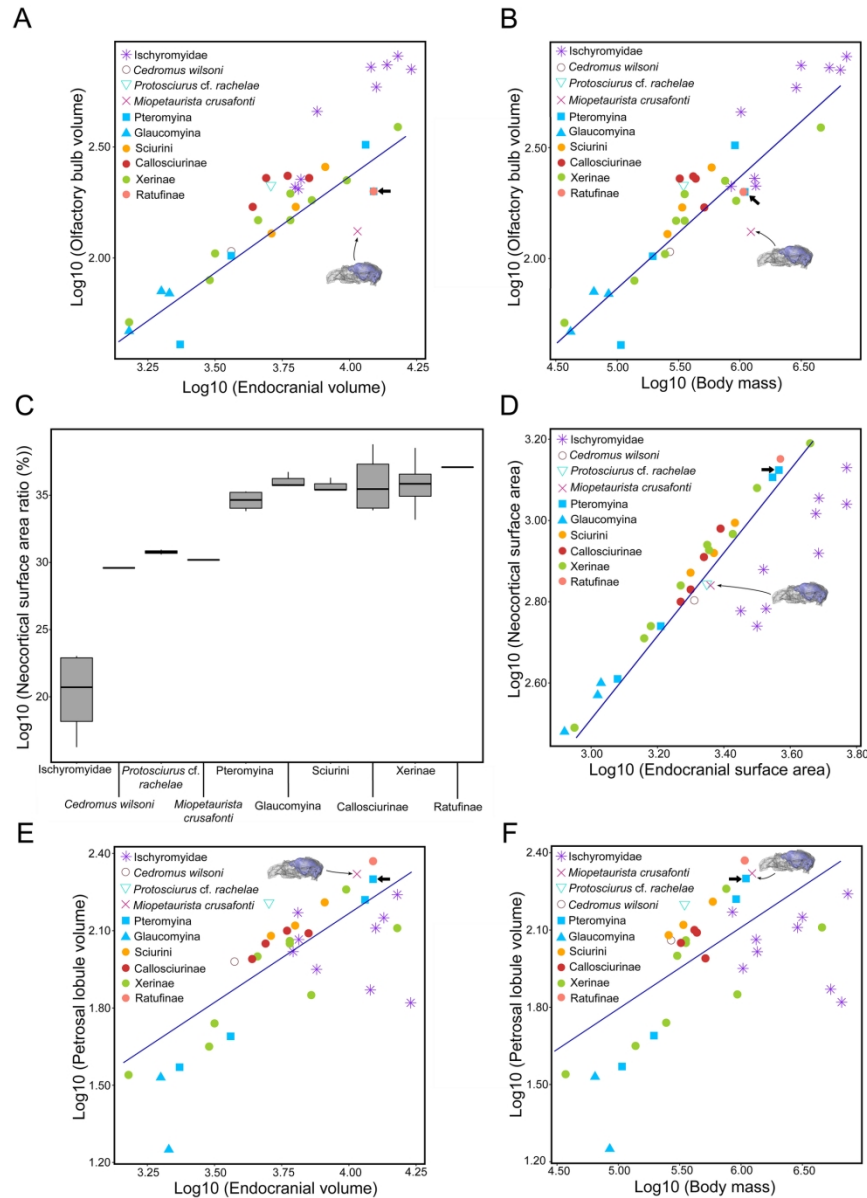


Fig. 9. Bivariate plots and boxplots for endocast measurements in Ischyromyidae and extant and extinct Sciuridae. A, bivariate plot of log 10 (olfactory bulb volume) versus log 10 (endocranial volume); B, bivariate plot of log 10 (olfactory bulb volume) versus log 10 (body mass); C, boxplot of neocortical surface area ratio; D, bivariate plot of log 10 (neocortical surface area) versus log 10 (endocranial surface area); E, bivariate plot of log 10 (petrosal lobule volume) versus log 10 (endocranial volume); F, bivariate plot of log 10 (petrosal lobule volume) versus log 10 (body mass). Phylogenetic generalized least-square (PGLS) regression lines are included for extant Sciuridae. The position of *Miopetaurista crusafonti* SNSB 1978 V 1 from Gumpersdorf as well as that of the extant *Petaurista petaurista* (thick arrow) is indicated in figures (A–B) and (D–F). PGLS regression results are given in Table 4. Residuals associated with the different PGLS regressions are given in Grau-Camats et al. (2021, table S6). Body mass, olfactory bulb, petrosal lobule and endocast volume (in mm³) and neocortical surface area for *Miopetaurista crusafonti* and other extinct and extant sciurid and ischyromyid rodents are given in Grau-Camats et al. (2021, table S4).

165x223mm (300 x 300 DPI)

1
2
3
4
5
6
7
8
9
10
11
12
13
14
15
16
17
18
19
20
21
22
23
24
25
26
27
28
29
30
31
32
33
34
35
36
37
38
39
40
41
42
43
44
45
46
47
48
49
50
51
52
53
54
55
56
57
58
59
60

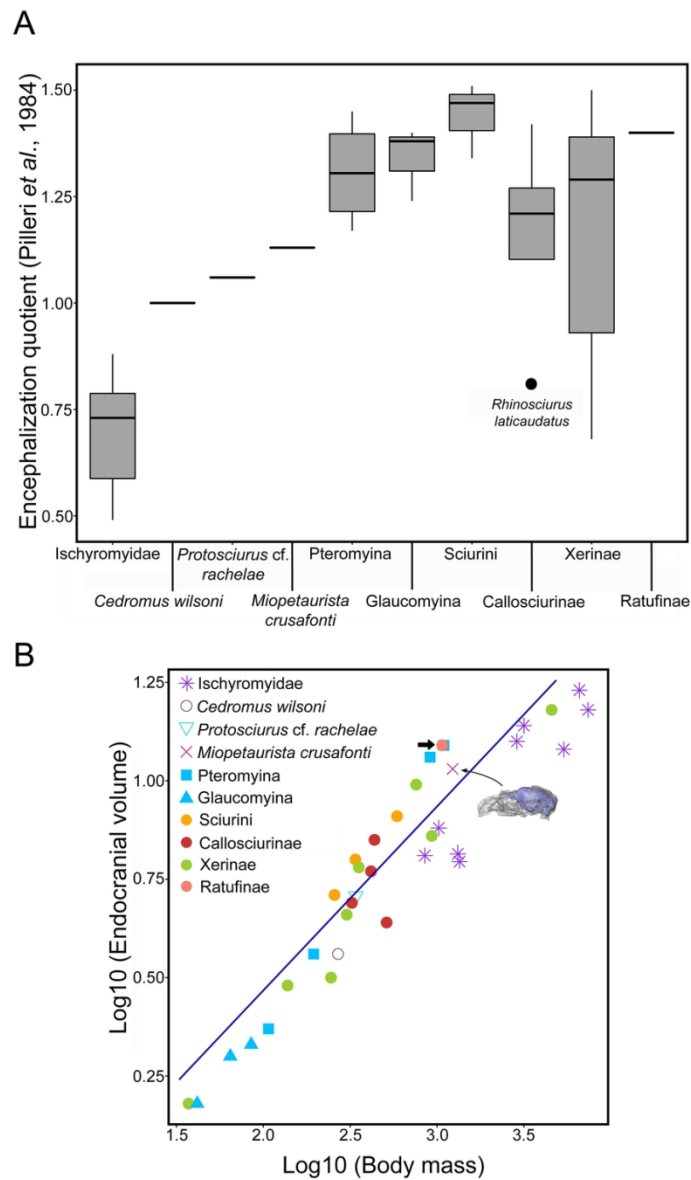


Fig. 10. Relationship between endocranial volume and body mass and encephalization quotients for extinct and extant Sciuridae and Ischyromyidae (see Table 1). A, Boxplot of EQs based on the equation by Pilleri et al. (1984). B, Bivariate plot of log 10 (endocranial volume) versus log 10 (body mass) for Sciuridae and Ischyromyidae. Phylogenetic generalised least-square (PGLS) regression line is included for extant Sciuridae. The position of *Miopetaurista crusafonti* SNSB 1978 V 1 from Gumpersdorf, as well as that of the extant *Petaurista petaurista* (thick arrow) is indicated in figure B. PGLS regression results are given in Table 4. Residuals associated with the different PGLS regressions are given in Grau-Camats et al. (2021, table S7). Body mass and endocast volume (in mm³) for *Miopetaurista crusafonti* and other extinct and extant sciurid and ischyromyid rodents are given in Grau-Camats et al. (2021, table S4).

80x133mm (300 x 300 DPI)

TABLE 1. Cheek tooth measurements for *Miopetaurista crusafonti* 1978 V 1 from Gumpersdorf.

<footnote>l, left side; r, right side. All measurements in mm.</footnote>

Element	Length	Width
P3 l	2.49	2.27
P4 l	3.97	4.05
M1 l	3.65	4.51
M2 l	3.72	4.44
M3 l	3.62	3.9
P3 r	2.37	2.16
M1 r	3.54	4.46
M2 r	3.79	4.42
M3 r	3.73	3.99

1
2
3
4
5 **TABLE 2.** Cranial measurements for extinct and extant flying squirrels as compared to *Miopetaurista crusafonti* 1978 V 1 from Gumpersdorf and
6
7
8 other extant and extinct flying squirrels.
9

10
11 <footnote>Cranial measurements for the virtually reconstructed skull of *M. neogrivensis* are after Casanovas-Vilar *et al.* (2018). Acronyms and
12
13 definitions of the measurements follow Nicolas *et al.* (2008) and Bertrand *et al.* (2016a): BNAS, maximum breadth of the nasals; BRCA, maximum
14
15 breadth of the braincase; BULL, maximum length of the auditory bulla; CTL, length of the upper cheek tooth row; DIA, length of the diastema
16
17 (from the alveolus of the incisor to the alveolus of the P3); HEBA, henselion–basion length; HEPA, henselion–palation length; IF, length of the
18
19 incisive foramen; INTE, smallest interorbital breadth; LNAS, maximum length of the nasals; PALA, smallest palatal breadth; RB, maximum
20
21 rostrum breadth; RH, mediosagittal projection of rostrum height at the anterior border of the M1; SL, maximum length of the skull. All
22
23 measurements are in mm. Estimated measurements (due to breakage or distortion) are given in parentheses; ‘>’ indicates that the measurement
24
25 could not be reliably taken but certainly exceeded the reported value.</footnote>
26
27
28
29
30
31
32
33
34
35
36
37
38
39
40
41
42
43
44
45
46

Species and specimen	SL	HEBA	HEPA	IF	DIA	INTE	ZYGO	PALA	CTL	ZYPL	BNAS	LNAS	BULL	BRCA	RH	RB
<i>Miopetaurista crusafonti</i> (1978 V1)	(67.7)	(59.4)	(36.0)	–	>14.7	(9.7)	–	7.3	17.0	8.6	–	–	–	(27.6)	>19.4	>12.1
<i>Miopetaurista neogrivensis</i> (IPS56468h)	(72.4)	(58.6)	(38.8)	6.8	16.1	(20.1)	–	(9.0)	18.4	(8.6)	–	>25.0	19.0	(30.3)	(22.7)	(20.0)
<i>Miopetaurista neogrivensis</i> (IPS88677)	(73.6)	(61.8)	38.1	6.9	17.8	–	(54.6)	(11.2)	17.4	11.3	–	>22.0	(18.9)	(37.2)	(24.1)	(21.7)
<i>Miopetaurista neogrivensis</i> (virtual recons.)	69.8	(58.8)	39.4	6.8	16.4	19.6	46.4	9.5	18.4	10.4	–	>19.2	19.0	37.2	25.1	(23.8)
<i>Petaurista petaurista</i> (ZMA131418)	64.5	54.1	30.7	3.3	12.7	16.7	44.8	7.3	15.5	5.9	12.0	19.4	13.2	29.7	20.2	14.5
<i>Eupetaurus cinereus</i> (19524)	72.3	58.5	35.7	6.2	14.7	18.7	44.1	12.0	19.6	9.0	13.0	24.7	14.7	26.7	23.9	13.8
<i>Aeromys tephromelas</i> (24076)	66.0	53.8	27.6	5.3	15.6	14.2	40.7	8.4	12.3	7.7	11.3	17.2	15.1	31.0	22.0	15.2
<i>Belomys pearsonii</i> (56.046)	43.2	34.3	20.8	2.9	9.3	8.5	26.0	4.8	9.9	4.4	6.4	13.1	10.2	20.1	12.7	8.4
<i>Pteromys volans</i> (40035)	36.5	29.4	15.9	4.3	7.5	9.9	22.6	5.4	6.6	4.6	6.1	11.6	10.5	16.4	11.8	6.4
<i>Hylopetes sagitta</i> (15512)	35.8	20.4	15.8	2.2	7.9	11.3	20.3	4.9	7.3	4.2	5.4	9.7	8.6	16.9	10.9	7.7
<i>Glaucomys volans</i> (19786)	34.4	28.3	16.0	2.0	7.3	8.3	20.8	4.7	6.3	4.4	5.0	10.0	9.8	15.7	10.4	7.4
<i>Glaucomys sabrinus</i> (IPS60584)	39.2	31.3	19.1	2.1	9.5	7.6	23.7	4.5	7.5	4.4	5.7	11.8	9.5	18.3	12.0	7.9
<i>Iomys horsfieldii</i> (15937)	30.5	23.8	15.7	1.1	5.7	8.3	19.1	5.1	7.2	2.8	4.8	8.3	7.4	15.7	8.6	7.2

1
2
3
4
5
6
7
8
9
10
11
12
13
14
15
16
17
18
19
20
21
22
23
24
25
26
27
28
29
30
31
32
33
34
35
36
37
38
39
40
41
42
43
44
45
46

TABLE 3. Endocranial volume, olfactory bulb, petrosal lobules, neocortical ratios and encephalization quotients for *Miopetaurista crusafronti* and published extant Pteromyini (Bertrand *et al.* 2017).

<footnote>We used the formula $NS1 \times 2 / TS$ to calculate the neocortical surface area ratio. Volume and surface area ratios are expressed as percentages. Encephalization quotients were calculated using the equations of Eisenberg (1981) and Pilleri *et al.* (1984).</footnote>

Subtribe	Species and specimen	Total endocranial volume (cm ³)	Neocortical surface area ratio (%) NS1×2/TS	Olfactory bulb volume ratio (%)	Petrosal lobule volume ratio (%)	EQ (Eisenberg 1981)	EQ (Pilleri <i>et al.</i> 1984)
Pteromyina	<i>Miopetaurista crusafronti</i> (1978 V1)	10.82	30.19	1.21	1.92	1.01	1.13
Pteromyina	<i>Aeromys tephromelas</i> (USNM 481190)	11.46	35.19	2.85	1.45	1.35	1.45
Pteromyina	<i>Petaurista petaurista</i> (USNM 589079)	12.32	35.28	1.64	1.62	1.25	1.38
Pteromyina	<i>Pteromyscus pulverulentus</i> (USNM 481178)	3.62	33.82	2.81	1.37	1.32	1.23
Pteromyina	<i>Pteromys volans</i> (USNM 172622)	2.33	34.11	1.75	1.61	1.33	1.17
Glaucomyina	<i>Glaucomyys volans</i> (AMNH 240290)	2.01	35.69	3.49	1.68	1.68	1.40
Glaucomyina	<i>Hylopetes spadiceus</i> (USNM 488639)	2.12	36.73	3.30	0.85	1.44	1.24
Glaucomyina	<i>Petinomys setosus</i> (USNM 488674)	1.51	35.76	3.10	-	1.73	1.38

TABLE 4. Phylogenetic generalized least-square linear regressions (PGLS) for endocast measurements and for total endocranial volume vs body size in our sample (see Figs 9, 10).

<footnote>For each regression, the values for the intercept, slope and associated significance, Pagel's λ , the pooled estimate of the residual standard error (RSE), degrees of freedom (df) for the model and residuals, 95 % confidence intervals for the slope (CI), and correlation coefficient (R^2) obtained from predicted and residual values. Residuals associated with the different regressions are provided in Grau-Camats *et al.* (2022, tables S6–S7). Body mass, olfactory bulb, petrosal lobule and endocast volume (in mm^3) as well as neocortical surface area for *Miopetaurista crusafonti* and other extinct and extant sciurid and ischyromyid rodents are given in Grau-Camats *et al.* (2022, table S4).</footnote>

Equation	intercept	slope	p-value (slope)	λ	RSE	df	95% CI	R^2 (predicted)	R^2 (residuals)
Log (olfactory bulb volume) / Log (endocranial volume)	1.462	0.928	0.000	0.937	0.181	36, 34	[0.808, 1.049]	0.909	0.885
Log (olfactory bulb volume) / Log (body mass)	0.852	0.509	0.000	0.611	0.150	36, 34	[0.427, 0.592]	0.865	0.856
Log (neocortical surface area) / Log (endocranial surface area)	-0.405	0.981	0.000	1.014	0.111	36, 34	[0.923, 1.039]	0.939	0.905
Log (neocortical surface area) / Log (endocranial surface area) [excluding Ischyromyidae]	-0.430	0.998	0.000	-0.094	0.018	24, 22	[0.960, 1.036]	0.993	0.992
Log (petrosal lobule volume) / Log (endocranial volume)	-0.666	0.708	0.000	0.352	0.181	35, 33	[0.482, 0.933]	0.590	0.557
Log (petrosal lobule volume) / Log (body mass)	0.3461	0.292	0.006	0.396	0.221	35, 33	[0.151, 0.434]	0.401	0.356
Log (endocranial volume) / Log (body mass)	-0.531	0.488	0.000	0.429	0.104	36, 34	[0.427, 0.549]	0.897	0.889

1
2
3
4
5
6
7
8
9
10
11
12
13
14
15
16
17
18
19
20
21
22
23
24
25
26
27
28
29
30
31
32
33
34
35
36
37
38
39
40
41
42
43
44
45
46

8